nature cell biology

Control of intestinal stem cell function and proliferation by mitochondrial pyruvate metabolism

John C. Schell[1], Dona R. Wisidagama[2], Claire Bensard[1], Helong Zhao[3], Peng Wei[1], Jason Tanner[1], Aimee Flores[4,5], Jeffrey Mohlman[6], Lise K. Sorensen[3], Christian S. Earl[1], Kristofor A. Olson[1], Ren Miao[1], T. Cameron Waller[1], Don Delker[7], Priyanka Kanth[7], Lei Jiang[8,9], Ralph J. DeBerardinis[8], Mary P. Bronner[6], Dean Y. Li[3], James E. Cox[1], Heather R. Christofk[4,10], William E. Lowry[4,5], Carl S. Thummel[2] and Jared Rutter[1,11,12]

Most differentiated cells convert glucose to pyruvate in the cytosol through glycolysis, followed by pyruvate oxidation in the mitochondria. These processes are linked by the mitochondrial pyruvate carrier (MPC), which is required for efficient mitochondrial pyruvate uptake. In contrast, proliferative cells, including many cancer and stem cells, perform glycolysis robustly but limit fractional mitochondrial pyruvate oxidation. We sought to understand the role this transition from glycolysis to pyruvate oxidation plays in stem cell maintenance and differentiation. Loss of the MPC in *Lgr5*-EGFP-positive stem cells, or treatment of intestinal organoids with an MPC inhibitor, increases proliferation and expands the stem cell compartment. Similarly, genetic deletion of the MPC in *Drosophila* intestinal stem cells also increases proliferation, whereas MPC overexpression suppresses stem cell proliferation. These data demonstrate that limiting mitochondrial pyruvate metabolism is necessary and sufficient to maintain the proliferation of intestinal stem cells.

It was first observed almost 100 years ago that, unlike differentiated cells, cancer cells tend to avidly consume glucose, but not fully oxidize the pyruvate that is generated from glycolysis[1]. This was originally proposed to be due to dysfunctional or absent mitochondria, but it has become increasingly clear that mitochondria remain functional and critical. Mitochondria are particularly important in proliferating cells because essential steps in the biosynthesis of amino acids, nucleotide and lipid occur therein[2–5]. Most proliferating stem cell populations also exhibit a similar glycolytic metabolic program[6–9], which transitions to a program of mitochondrial carbohydrate oxidation during differentiation[10,11]. The first distinct step in carbohydrate oxidation is import of pyruvate into the mitochondrial matrix, where it gains access to the pyruvate dehydrogenase complex (PDH) and enters the tricarboxylic acid (TCA) cycle as acetyl-CoA. We, and others, recently discovered the two proteins that assemble to form the mitochondrial pyruvate carrier (MPC)[12,13]. This complex is necessary and sufficient for mitochondrial pyruvate import in yeast, flies and mammals, and thereby serves as the junction between cytoplasmic glycolysis and mitochondrial oxidative phosphorylation. We previously showed that decreased expression and activity of the MPC underlies the glycolytic program in colon cancer cells *in vitro* and that forced re-expression of the MPC subunits increased carbohydrate oxidation and impaired the ability of these cells to form colonies *in vitro* and tumours *in vivo*[14]. This impairment of tumorigenicity was coincident with a loss of key markers and phenotypes associated with stem cells. This prompted us to examine whether glycolytic non-transformed stem cells might also exhibit low MPC expression and mitochondrial pyruvate oxidation, which must increase during differentiation.

RESULTS

MPC expression is low in intestinal stem cells and increases following differentiation

As a model system, we have studied LGR5^{+} intestinal stem cells (ISCs), which reside near the base of the intestinal crypt and continuously proliferate. Their progeny differentiate and populate the

[1]Department of Biochemistry, University of Utah School of Medicine, Salt Lake City, Utah 84112, USA. [2]Department of Human Genetics, University of Utah School of Medicine, Salt Lake City, Utah 84112, USA. [3]Department of Molecular Medicine, University of Utah School of Medicine, Salt Lake City, Utah 84112, USA. [4]Eli and Edythe Broad Center for Regenerative Medicine, University of California Los Angeles, Los Angeles, California 90095, USA. [5]Department of Molecular Cell and Developmental Biology, University of California Los Angeles, Los Angeles, California 90095, USA. [6]Department of Pathology, University of Utah School of Medicine, Salt Lake City, Utah 84112, USA. [7]Department of Internal Medicine, University of Utah School of Medicine, Salt Lake City, Utah 84112, USA. [8]Children's Medical Center Research Institute, University of Texas Southwestern Medical Center, Dallas, Texas 75390, USA. [9]Department of Molecular and Cellular Endocrinology, Beckman Research Institute at City of Hope, Duarte, California 91010, USA. [10]Department of Biological Chemistry, University of California Los Angeles, Los Angeles, California 90095, USA. [11]Howard Hughes Medical Institute, University of Utah School of Medicine, Salt Lake City, Utah 84112, USA.
[12]Correspondence should be addressed to J.R. (e-mail: rutter@biochem.utah.edu)

Received 4 October 2016; accepted 18 July 2017; published online 14 August 2017; DOI: 10.1038/ncb3593

intestinal epithelium, which is completely renewed approximately every 5 days[15,16]. Using EGFP fluorescence from an *Lgr5*-EGFP-IRES-CreERT2 allele, we single-cell-sorted intestinal crypt stem cells into low-, medium- and high-LGR5-expressing populations (Supplementary Fig. 1a). As expected *Lgr5* messenger RNA, as well as that of other markers of stem cells, correlated with *Lgr5*-EGFP expression, while *Krt20* and other markers of differentiation anti-correlated with EGFP (Fig. 1a,b and Supplementary Table 1). The pattern of *Mpc1* and *Mpc2* expression resembled that of differentiation genes, exhibiting lower expression in the more stem-like cells that increased with differentiation. *In vitro* organoids maintained in stem cell or differentiation-promoting conditions displayed a similar pattern. When grown in basal medium containing EGF and Noggin, organoids exhibit a largely differentiated gene expression pattern, which is progressively more stem-like when R-spondin 1 and Wnt3a are added to the medium (Fig. 1c,d and Supplementary Table 2). Expression of *Mpc1* and, to a lesser extent, *Mpc2* again correlate with the expression of differentiation genes. Both *in vivo* and *in vitro*, the expression of indicators of mitochondrial biogenesis such as *Tfam* and *Nrf1* was higher in more stem-like cell populations (Fig. 1a–d) suggesting that the decreased MPC expression is not due to a global suppression of mitochondrial gene expression. Similarly, immunohistochemical analysis of the proximal small intestine (jejunum) revealed that MPC1 was nearly absent from the base of the crypt, the site of LGR5$^+$ ISCs, but strongly expressed through the upper crypt and villus, whereas VDAC, a marker of total mitochondrial mass, was more abundant at the base of the crypt relative to the remainder of the intestinal epithelium in both mouse and human (Fig. 1e). Similar anti-correlation of MPC1 and LGR5 expression was observed by immunofluorescence staining of small intestine (Fig. 1f). This pattern of MPC1 and VDAC expression was consistent throughout the murine small intestine (jejunum and ileum) and NRF1, TFAM and PDK1 were also more abundant in the crypt cells in human intestine while the differentiation mark CK20 was less abundant[17,18] (Supplementary Fig. 1b,c). Electron microscopy also showed high mitochondrial content in crypt stem cells, and isolated *Lgr5*-EGFP stem cells robustly stain with a dye dependent on mitochondrial membrane potential (Fig. 1g,h). These data are consistent with the hypothesis that crypt stem cells contain functional mitochondrial, but that they are geared toward biosynthetic activities or oxidation of fatty acids or other non-carbohydrate fuels.

Drosophila MPC regulates intestinal stem cell proliferation

These observations led us to hypothesize that the MPC plays an active and direct role in regulating ISC proliferation. To begin to test this hypothesis, we examined the role of the MPC in the ISCs of the fruit fly *Drosophila*, which share key aspects of their biology with mammalian ISCs[19,20]. Both MPC1 and MPC2 are expressed in all four cell types of the intestine, with the lowest level of expression in the ISCs and the highest expression in the differentiated enteroendocrine cells[21,22]. Confocal imaging of intestines dissected from *dMPC1* mutants revealed that the epithelium exhibits multilayering unlike the normal single-cell layer seen in controls (Fig. 2a). This is a classic overgrowth phenotype that is associated with oncogene mutations in *Drosophila*[20]. Accordingly, we used MARCM clonal analysis to determine whether a specific loss of the MPC in ISCs leads to an increase in their proliferation[23]. On average, newly divided GFP-marked *dMPC1* mutant clones are more than twofold larger than control clones, which were generated in parallel using a wild-type chromosome, indicating that the MPC is required in the ISC lineage to suppress proliferation (Fig. 2b and Supplementary Table 7). Because GFP-marked clones could include cells that differentiate into mature enterocytes or enteroendocrine cells, we also conducted clonal analysis in the absence of *Notch*, thereby blocking ISC differentiation[24,25]. Under these conditions, we again observed an approximately twofold increase in the size of *dMPC1* mutant ISC clones (Fig. 2c and Supplementary Table 7). To confirm and extend these results, we disrupted *MPC* function specifically in the ISCs by using the *Dl-GAL4* driver in combination with *UAS-GFP*, which facilitates stem cell identification. Once again, approximately twofold more GFP-marked stem cells were observed relative to controls when either *dMPC1* or *dMPC2* expression was disrupted by RNA-mediated interference (RNAi) along with increased ISC proliferation as detected by staining for phosphorylated histone H3 (pHH3) (Fig. 2d). Similar results were obtained when RNAi was targeted to the E1 or E2 subunits of PDH to specifically disrupt the next step in mitochondrial pyruvate oxidation (Fig. 2d and Supplementary Fig. 2a and Supplementary Table 7). Importantly, an opposite phenotype was seen when *Ldh* was reduced by RNAi in the ISCs or progenitor cells (Fig. 2e,f and Supplementary Fig. 2a and Supplementary Table 7). Ldh suppression is known to result in a significant increase in pyruvate levels, which can promote pyruvate oxidation[26]. Taken together with our results with *Pdh* RNAi, these observations support the model that the MPC limits stem cell proliferation through promoting oxidative pyruvate metabolism in the mitochondria. It also appears to be sufficient as specific overexpression of MPC1 and MPC2 in ISCs or progenitors caused a reduction in stem cell proliferation, the opposite of the loss-of-function phenotype. This can be seen in either *Pseudomonas*-infected intestines (Fig. 2e and Supplementary Fig. 2a), which undergo rapid stem cell proliferation[27], or under basal conditions in aged animals (Fig. 2f). Consistent with this, MPC overexpression under basal conditions had no effects on intestinal morphology, while the intestines from infected flies displayed a fully penetrant size reduction, which is probably due to the inability of ISCs to maintain tissue homeostasis (Fig. 2g and Supplementary Figs 2b and 7c). Taken together, our results demonstrate that mitochondrial pyruvate uptake and metabolism is both necessary and sufficient in a stem cell autonomous manner to regulate ISC proliferation and maintain intestinal homeostasis in *Drosophila*.

MPC deletion in the *Lgr5*-EGFP cells expands the intestinal stem cells compartment and increases proliferation

To test whether loss of the mammalian MPC might have similar effects on ISC homeostasis, we generated mice carrying the *Lgr5*-EGFP-IRES-CreERT2 allele together with homozygous floxed alleles of *Mpc1* (Supplementary Fig. 3a). Tamoxifen treatment resulted in a significant but incomplete (~30%) loss of MPC1 in the proximal small intestine at 30 days (Fig. 3a,f). Loss of *MPC1* had no effect on body weight and caused no change in the morphology or height of intestinal crypts or villi (Fig. 3a and Supplementary Figs 3b–d). We also observed no change in alcian blue staining, which marks goblet cells or perturbation in the mature enterocyte marker CK20 (Fig. 3a and Supplementary Fig. 3e). These animals exhibited,

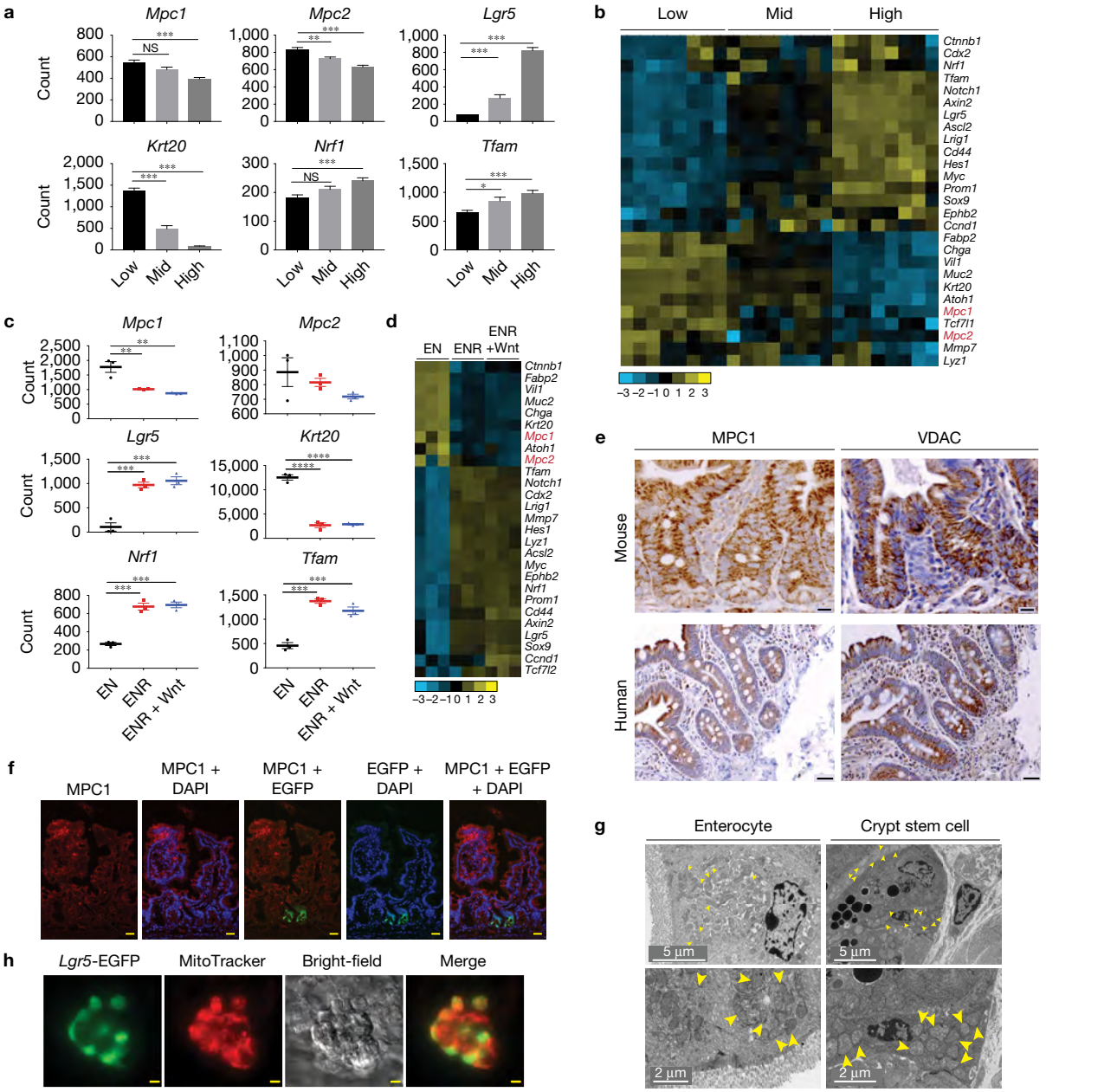

Figure 1 MPC expression is low in intestinal stem cells and increases following differentiation. (**a**) The indicated transcripts were quantified in *Lgr5*-EGFP cells sorted for low, mid and high EGFP intensity ($n = 13$, low and mid, $n = 12$ high). (**b**) Heat map of mRNA content from the *Lgr5*-EGFP populations in **a**. (**c**) The indicated transcripts were quantified from organoids transferred to differentiation conditions (EN: EGF and Noggin) compared with stem-maintaining conditions containing RSPO1 (ENR) or RSPO1 and Wnt3A (ENR + Wnt) ($n = 3$ per treatment). (**d**) Heat map of mRNA content from the organoids in **c**. (**e**) Antibody stain of MPC1 and VDAC on crypts of proximal small intestine in mouse (top) and human (bottom). (**f**) Immunofluorescence images of mouse proximal small intestine staining for MPC1 (red) and EGFP for *Lgr5* intestinal stem cells (green). (**g**) Electron micrographs of enterocytes (left) and crypt stem cells and surrounding Paneth cells (right) at low (top) and high (bottom) magnification. The yellow arrowheads indicate mitochondria. (**h**) Isolated live crypts imaged for *Lgr5*-EGFP and co-stained with MitoTracker Red CMXRos. Data are mean ± s.e.m. $^{*}P < 0.05$, $^{**}P < 0.01$, $^{***}P < 0.001$; NS, not significant. Scale bars, 50 µm (**e**, human; **h**) and 20 µm (**e**, mouse; **f**). *P* values for **a**,**c** were calculated by one-way ANOVA with correction for multiple comparisons.

however, a significant increase in the number and zone size of actively proliferating cells in the crypt as measured both by BrdU incorporation and Ki67 staining (Fig. 3b,c and Supplementary Fig. 3f). In addition, $Mpc1^{Lgr5\text{-}KO}$ mice had an increased number of crypt stem cells as assessed by *Olfm4*, *Lgr5* and LRIG1 expression as well as by expression of GFP from the *Lgr5*-EGFP allele (Fig. 3d,e and Supplementary Fig. 3g–i). Consistent with these data, we found that the zone of MPC1-deficiency increased over time post-*Mpc1* deletion, suggesting positive selection for *Mpc1*-deleted cells (Fig. 3f). These data support our results in *Drosophila* and demonstrate that $Mpc1^{Lgr5\text{-}KO}$ crypts display increased cell cycling and ISC expansion.

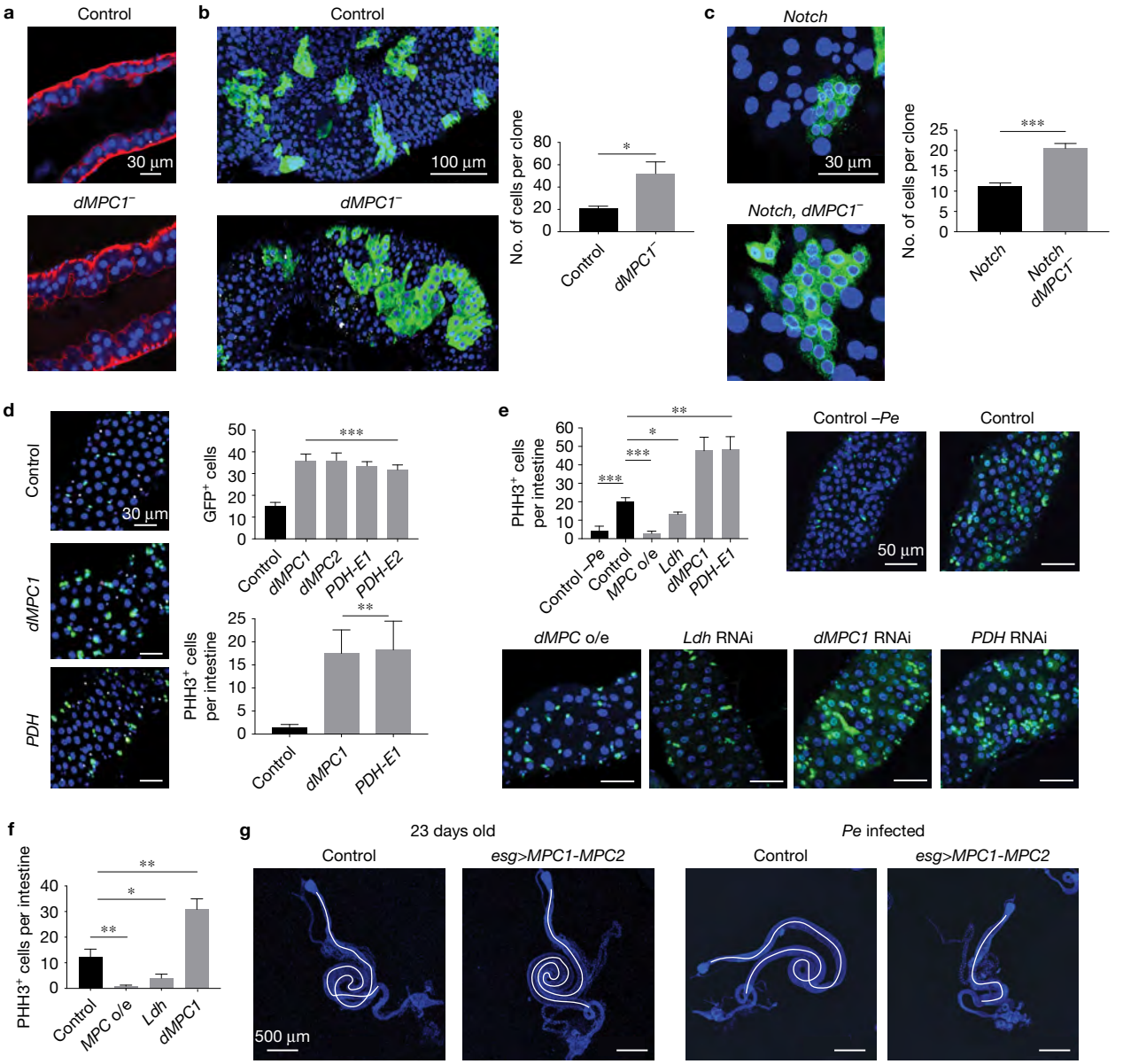

Figure 2 *Drosophila* MPC regulates intestinal stem cell proliferation. (**a**) Intestines from controls and *dMPC1* mutants stained with phalloidin (red) and DAPI (blue), ($n=10$ control, $n=7$ knockout). (**b**) MARCM *dMPC1* mutant clones marked by GFP along with quantification of clone size ($n=13$ clones from control, $n=12$ clones from knockout, 15 animals assessed for each group). (**c**) MARCM *dMPC1* mutant clones with *Notch* RNAi marked by GFP along with quantification ($n=31$ from control, $n=38$ from knockout). (**d**) *Dl-GAL4* used to target RNAi as indicated, (control $n=8$, *dMPC1* RNAi $n=8$, *dMPC2* RNAi $n=8$, *PDH-E1* $n=7$, *PDH-E2* $n=7$ experimental replicates). Increased proliferation as detected by staining for phosphorylated histone H3 (pHH3) (PHH3 + cells counted from control $n=8$, *dMPC1* RNAi $n=8$, *PDH-E1* $n=7$). (**e**) *Dl-GAL4* used to target RNAi as indicated or *MPC* overexpression (o/e) under infected conditions (control $n=5$ (no infection), control with infection $n=10$, *dMPC* o/e $n=10$, *Ldh* RNAi $n=10$, *dMPC1* RNAi $n=10$, *PDH* RNAi $n=10$). (**f**) *esg-GAL4* was used to direct *MPC* overexpression (o/e) or RNAi targeting *Ldh* or *dMPC1* under uninfected basal conditions in 23-day-old adults maintained at 29 °C (control $n=10$, *MPC* o/e $n=10$, *Ldh* RNAi $n=10$, *dMPC1* RNAi $n=10$). (**g**) Intestine size is unaffected in animals overexpressing *MPC* under basal conditions in aged flies (left two panels) and reduced in infected animals (right two panels) ($n=10$ for control and *MPC* o/e). Data are mean ± s.e.m. $^{*}P<0.05$, $^{**}P<0.01$, $^{***}P<0.001$. All *P* values were calculated using Student's *t*-test. *Pe*, *Pseudomonas entomophila*.

In vitro loss of the MPC increases stem cell function and organoid formation

A dramatic increase in organoid-forming potential was observed after plating crypts isolated from $Mpc1^{Lgr5\text{-}KO}$ mice, supporting the conclusion that these animals have an enlarged population of proliferating ISCs (Fig. 4a and Supplementary Table 7). Similar results were seen when organoids were established from single $Lgr5^{+}$ stem cells treated with tamoxifen *in vitro* to eliminate MPC1 (Fig. 4b and Supplementary Table 7), exhibiting more *Lgr5*-EGFP-positive branches (Fig. 4c). When cells from these organoids were dissociated and sorted, $Mpc1^{Lgr5\text{-}KO}$ organoids maintained a higher fraction of GFP-positive cells (Fig. 4d and Supplementary Fig. 4a

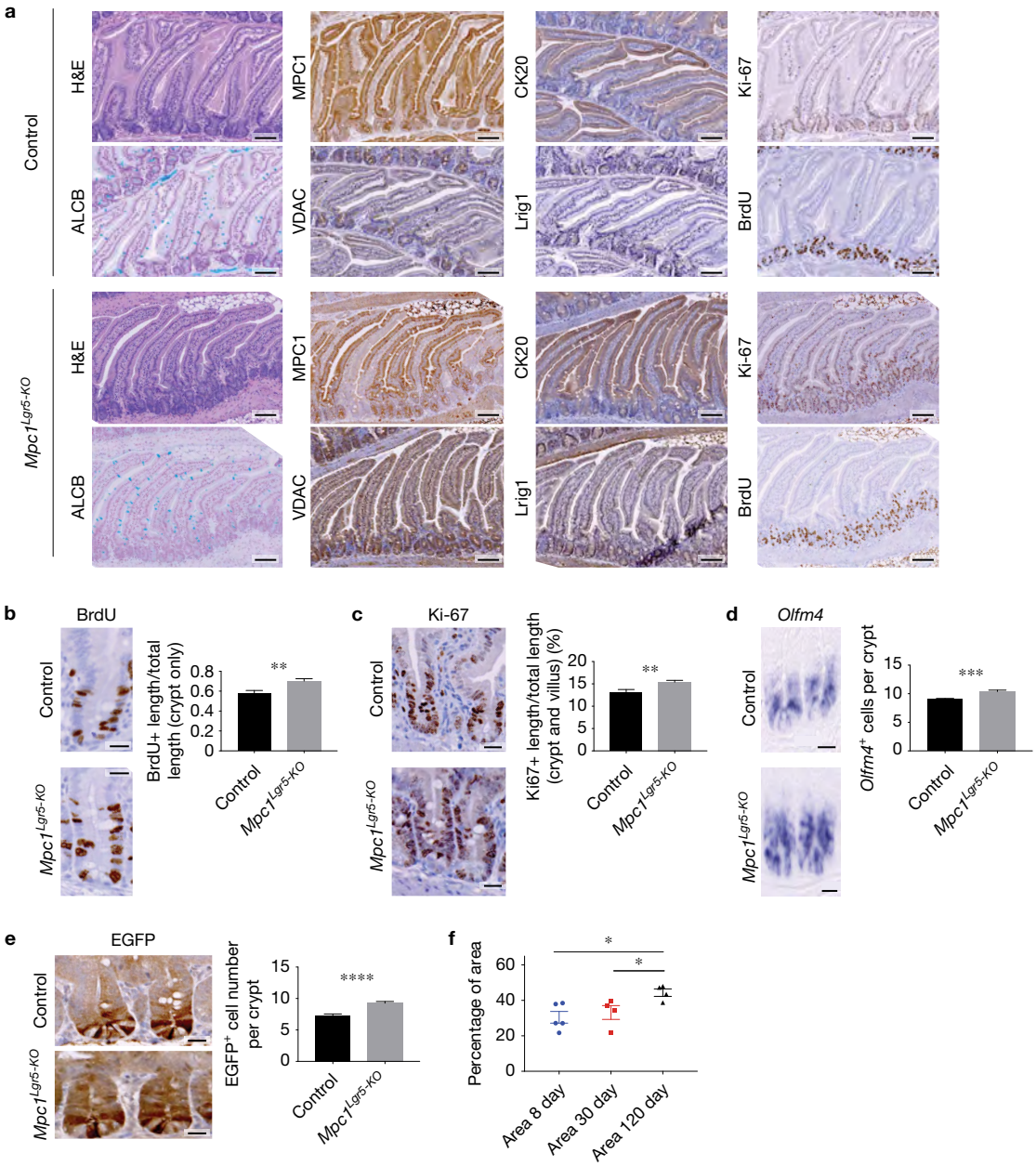

Figure 3 MPC deletion in the *Lgr5*-EGFP compartment increases intestinal stem cell maintenance and proliferation. (**a**) Images of haematoxylin and eosin (H&E), MPC1, CK20, Ki-67, alcian blue, VDAC, Lrig1 and BrdU staining in control and $Mpc1^{Lgr5\text{-}KO}$ proximal small intestine. (**b**) Representative images and quantification of BrdU stained crypt nuclei in control and $Mpc1^{Lgr5\text{-}KO}$ animals ($n=9$ control, $n=10$ knockout). (**c**) Representative images and quantification of Ki-67-positive nuclei in crypts of control and $Mpc1^{Lgr5\text{-}KO}$ animals ($n=9$ control, $n=10$ knockout). (**d**) Representative images of *Olfm4 in situ* hybridization of control and $Mpc1^{Lgr5\text{-}KO}$ small intestine with quantification of positive cells per crypt (right) ($n=9$ control and knockout). (**e**) Images of GFP-stained cells in control and $Mpc1^{Lgr5\text{-}KO}$ animals with quantification of GFP-positive cells per crypt ($n=9$ control and knockout). (**f**) Percentage of area of proximal small intestine without MPC1 by immunohistochemistry in animals 8, 30 and 160 days post-tamoxifen treatment ($n=5$ for 8 and 30 day, $n=4$ for 160 day). Data are mean ± s.e.m. $^{*}P<0.05$, $^{**}P<0.01$, $^{***}P<0.001$, $^{****}P<0.0001$. Scale bars, 100 μm (**a**) and 20 μm (**b**–**e**). All *P* values were calculated using Student's *t*-test.

and Supplementary Table 7). When cells from these wild-type and $Mpc1^{Lgr5\text{-}KO}$ organoids were dissociated, but not sorted for EGFP, those from $Mpc1^{Lgr5\text{-}KO}$ organoids maintained their increased organoid-forming ability (Fig. 4e) and were more likely to be *Lgr5*-EGFP-positive (Fig. 4f). This increase in organoid formation of single $Mpc1^{Lgr5\text{-}KO}$ cells was maintained over extended passaging over two months (Supplementary Fig. 4b). Moreover, $Mpc1^{Lgr5\text{-}KO}$ organoids transferred to basal medium lacking the drugs that maintain stemness rapidly lost EGFP fluorescence, while $Mpc1^{Lgr5\text{-}KO}$ organoids retained significant EGFP expression surrounding the autofluorescent lumen (Fig. 4g).

In vitro loss of the MPC alters protein expression and metabolism

To further define the molecular effects of MPC loss, we isolated wild-type and $Mpc1^{Lgr5\text{-}KO}$ organoid populations and subjected them

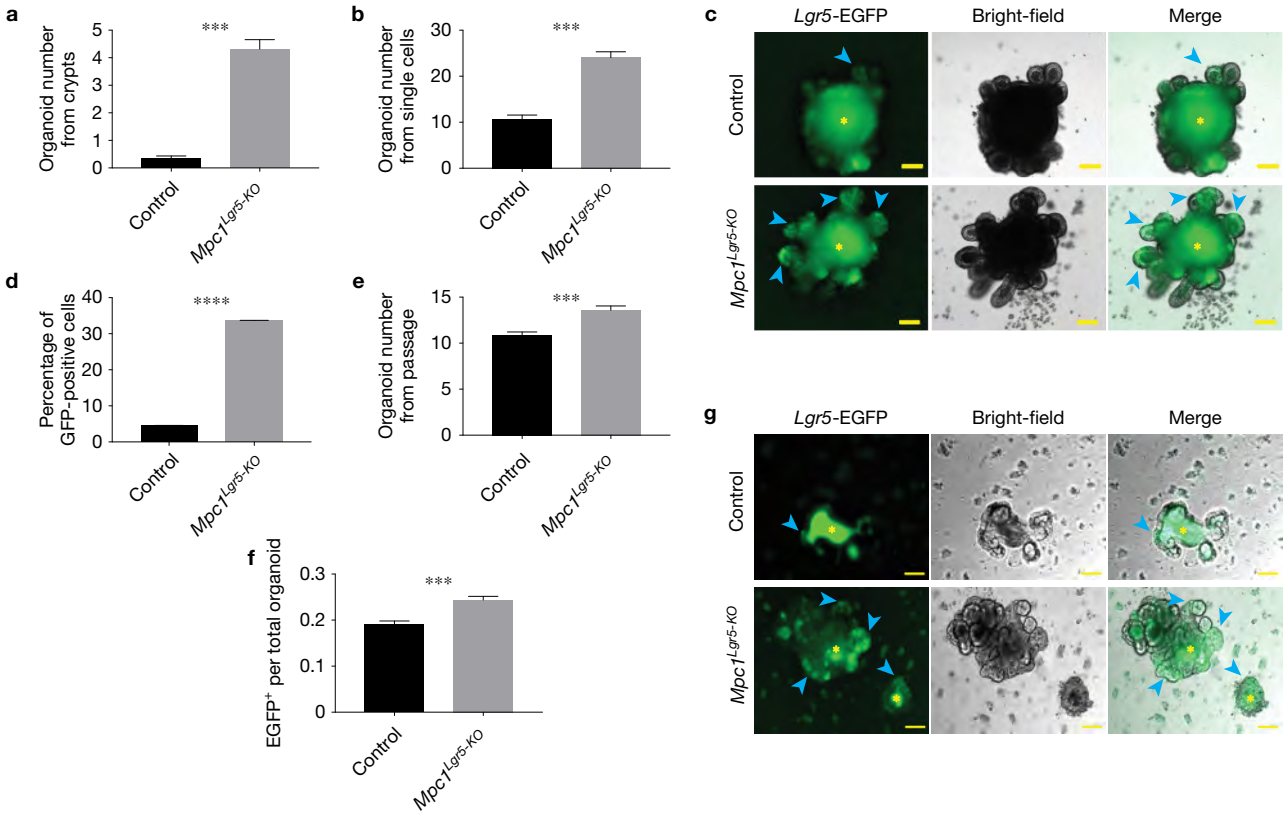

Figure 4 *In vitro* loss of the MPC increases stem cell function and organoid formation. (**a**) Quantification of organoid formation from intestinal crypts isolated from control and *Mpc1* knockout (KO) mice treated with tamoxifen ($n=3$ control, $n=4$ knockout animals with 10 separate organoid cultures from each animal). (**b**) Quantification of organoid formation from single *Lgr5*-EGFP^{+} cells from *Mpc1*$^{fl/fl}$ intestines after *in vitro* vehicle (control) or tamoxifen (KO) treatment ($n=20$ experimental replicates). (**c**) Images of mature organoids grown from the cells in **b**. The blue arrowheads indicate *Lgr5*-EGFP^{+} crypt domains and the yellow asterisks indicate autofluorescent lumens. (**d**) Flow cytometry for the cells in **b**, showing percentage of GFP-positive ($n=5$ control, $=6$ knockout). (**e**) Secondary organoid formation from single cells passaged from **b** as single live cells ($n=20$ experimental replicates). (**f**) Fraction of *Lgr5*-EGFP-expressing secondary organoids in control and *Mpc1* KO cultures ($n=20$ experimental replicates). (**g**) Images of control and *Mpc1* KO organoids following withdrawal of the stem-cell-maintaining drugs CHIR99021 and valproic acid (representative of two experiments). The blue arrowheads indicate *Lgr5*-EGFP^{+} cells and the yellow asterisks indicate autofluorescent lumens. Data are mean ± s.e.m. $^{***}P<0.001$, $^{****}P<0.0001$. Scale bars, 100 μm (**c**,**g**). All *P* values were calculated using Student's *t*-test.

to protein analysis. As expected, *Mpc1*-deleted organoids had an essentially complete loss of MPC1 protein, and a significant reduction in MPC2, which is dependent on MPC1 for its stability (Fig. 5a and Supplementary Figs 4c and 7a,d)[14,28–30]. Both the LGR5 and beta-catenin stem cell markers were elevated in *Mpc1*$^{Lgr5\text{-}KO}$ organoids (Fig. 5a and Supplementary Fig. 7), consistent with effects on the mRNAs encoding stem and differentiation marks (Supplementary Fig. 4d and Supplementary Table 3). We also observed that histone acetylation, and specifically H3K27 and H3K4 acetylation marks, were decreased in *Mpc1*-deleted organoids (Fig. 5b and Supplementary Figs 4e and 7b). As expected, *Mpc1*$^{Lgr5\text{-}KO}$ organoids exhibited a steady-state increase in pyruvate and a decrease in citrate, malate and alpha-ketoglutarate, consistent with a failure of cytoplasmic pyruvate to enter the mitochondrial TCA cycle (Fig. 5c and Supplementary Fig. 4f). *Mpc1*$^{Lgr5\text{-}KO}$ organoids also showed a significant impairment in flux of ^{13}C-glucose into the TCA cycle as measured by M+0 loss and M+2 accrual in the citrate pool (Fig. 5d and Supplementary Table 7). Oxygen consumption was also markedly impaired under both basal and FCCP-stimulated (maximal) conditions in both *Mpc1*$^{Lgr5\text{-}KO}$ organoids and wild-type organoids treated with UK-5099, which is a specific and efficacious MPC inhibitor[12,13,31] (Fig. 5e). No further decrease in oxygen consumption was observed when *Mpc1*$^{Lgr5\text{-}KO}$ organoids were treated with the inhibitor. This led us to explore whether fatty acid oxidation might be increased to compensate for loss of *Mpc1*-dependent carbohydrate oxidation. In fact, we found that etomoxir-sensitive respiration (that is, fatty acid oxidation) was profoundly increased by either inhibition or genetic deletion of MPC function (Fig. 5f).

In vitro inhibition of MPC activity increases organoid formation

In addition to genetically MPC-deficient organoids, we next utilized the MPC inhibitor UK-5099 to examine the effects of acute MPC loss. Similar to *Mpc1*$^{Lgr5\text{-}KO}$ organoids, we found that treatment of crypt-derived organoids with UK-5099 led to enhanced maintenance of EGFP expression in the epithelial lining (Fig. 6a) and a larger number of crypt-like branches per organoid, indicative of increased stem cell activity (Fig. 6b and Supplementary Table 7). We also observed that UK-5099 treatment caused an approximately fourfold increase in the efficiency of organoid formation from proximal small intestine (Fig. 6c and Supplementary Table 7). When treated organoids were dissociated

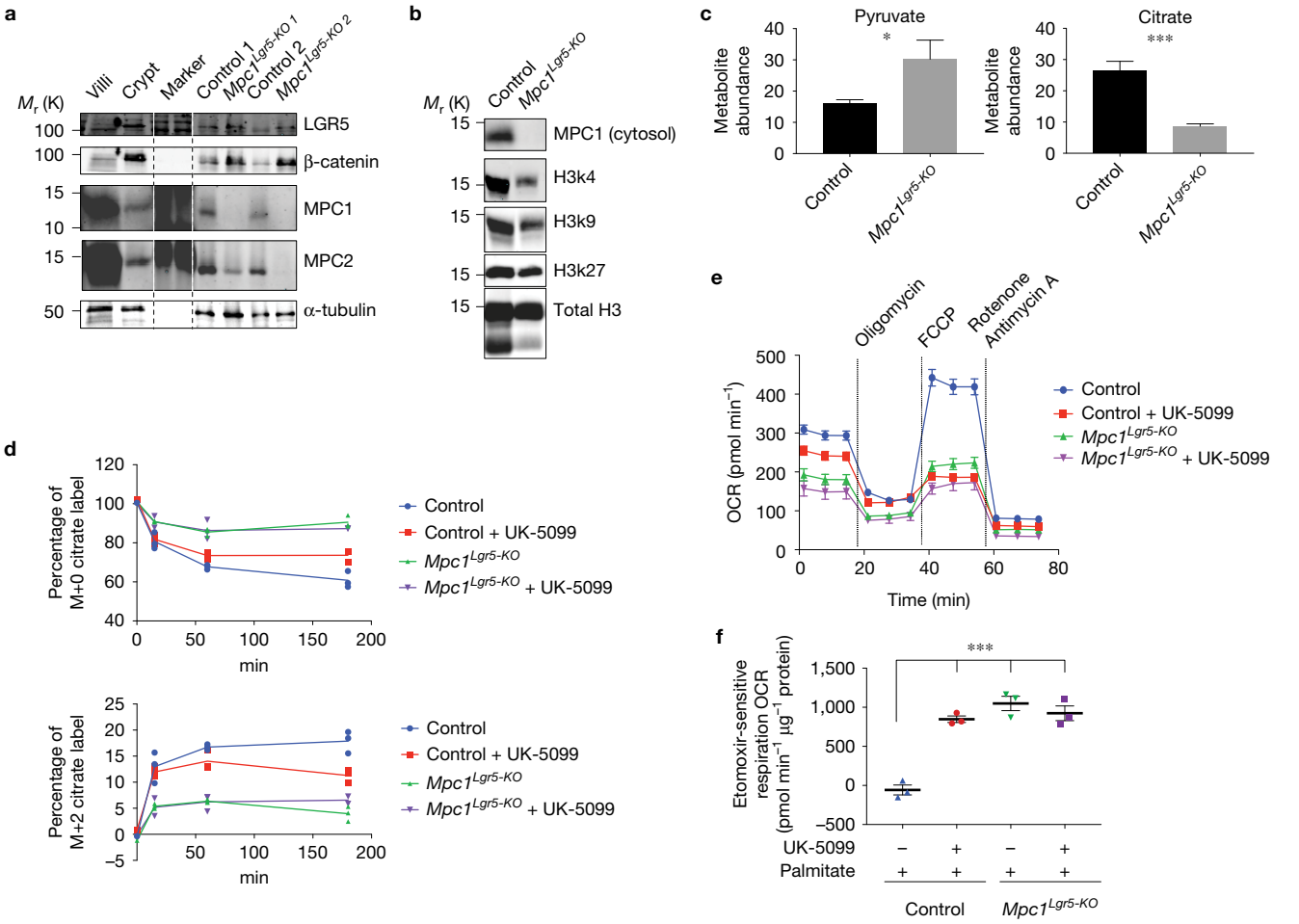

Figure 5 *In vitro* loss of the MPC alters protein expression and metabolism. (**a**) Immunoblot of replicate control and *Mpc1*$^{Lgr5\text{-}KO}$ organoid cultures with villi and crypt extract as negative and positive controls respectively. (**b**) Immunoblot on isolated nuclei from control and *Mpc1*$^{Lgr5\text{-}KO}$ organoids for acetyl histone 3 marks. (**c**) Steady-state abundance of citrate and pyruvate in control and *Mpc1*$^{Lgr5\text{-}KO}$ organoids ($n=6$ experimental replicates). (**d**) Flux metabolic labelling of citrate (M+0 on top, M+2 on bottom) at the indicated times following U-^{13}C-glucose addition in control and *Mpc1*$^{Lgr5\text{-}KO}$ organoids with and without UK-5099 treatment ($n=1$ for 0 h per condition and $n=3$ for each additional time point). (**e**) Oxygen consumption rate (OCR) of control and *Mpc1* KO organoids with and without UK-5099 utilizing glucose for respiration ($n=8$ experimental replicates). (**f**) Etomoxir-sensitive oxygen consumption of control and *Mpc1*$^{Lgr5\text{-}KO}$ organoids with and without UK-5099 treatment utilizing palmitate for respiration ($n=3$ experimental replicates). Data are mean ± s.e.m. $^{*}P<0.05$, $^{***}P<0.001$. All P values were calculated using Student's t-test. Unprocessed original scans of western blots are shown in Supplementary Fig. 7.

and assessed by flow, UK-5099 treatment significantly increased the percentage of GFP-positive cells (Fig. 6d and Supplementary Table 7). MPC inhibition enhanced organoid formation from all regions of the small intestine and from the colon to a degree similar to that of the canonical organoid-maintaining condition containing valproic acid and CHIR99021 (Supplementary Fig. 5a). We also observed that human colon organoid colony formation and growth was promoted by UK-5099 treatment (Fig. 6e and Supplementary Table 7).

Interestingly, organoids could be maintained for at least one year of continuous UK-5099 treatment and they continued to display an increase in crypt domains per organoid (Fig. 6f). The addition of UK-5099 also improved passaging efficiency of early crypts (Supplementary Fig. 5b). When organoids were transferred to differentiation conditions, treatment with UK-5099 resulted in maintenance of *Lgr5*-EGFP expression in the crypt domains (Fig. 6g). Similarly, when removing stem-cell-maintaining factors and allowing passive differentiation, UK-5099 delayed the emergence of highly autofluorescent organoid lumens, suggesting fewer or lower activity of differentiated secretory cells (Supplementary Fig. 5c). We also examined the effect of MPC inhibition in comparison and combination with the HDAC inhibitor valproic acid and/or the GSK-3beta inhibitor CHIR99021, both of which promote stem cell maintenance independent of the Paneth cell niche[32]. UK-5099 and valproic acid caused a similar increase in organoid formation from crypts relative to controls, and resulted in a similar additive effect when combined with CHIR99021 (Fig. 6h and Supplementary Table 7) with each drug being used at its optimal concentration (Supplementary Fig. 5d). The GSK-3beta inhibitor had stronger effects than either of the other two drugs alone and was also additive with all other combinations. We conclude that MPC inhibition has profound effects on stem cell maintenance that are at least partially mechanistically distinct from those caused by HDAC or

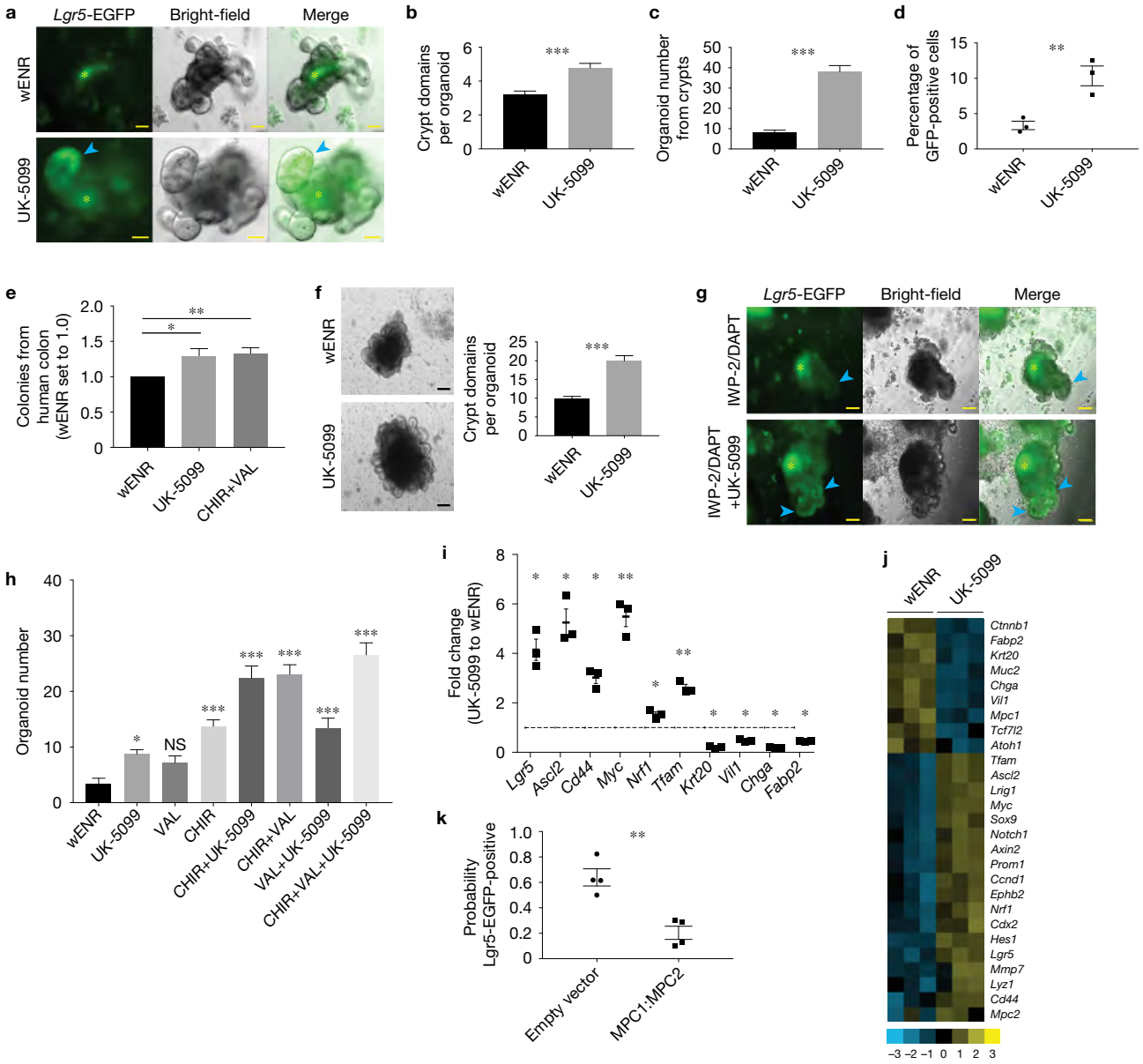

Figure 6 *In vitro* inhibition of MPC activity increases organoid formation. (**a**) Images of organoids from crypts with and without UK-5099. The blue arrowhead points to a *Lgr5*-EGFP^{+} crypt domain and the purple asterisks indicate autofluorescent lumens. (**b**) Quantification of crypt domains per organoid with and without UK-5099 ($n=6$ experimental replicates). (**c**) Quantification of organoid formation from crypts from proximal small intestine with and without UK-5099 ($n=16$ wENR, $n=14$ UK-5099 experimental replicates). (**d**) Flow cytometry for the cells in **c** showing the percentage of GFP-positive ($n=3$ replicates per condition). (**e**) Human ascending colon crypts treated with wENR basal medium (set to 1) or medium containing UK-5099 or CHIR99021 plus valproic acid (CHIR+VAL) ($n=5$ patients with 6–8 individual cultures per patient sample). (**f**) Representative images and quantification of crypt domains in organoids maintained with and without UK-5099 for 12 months (wENR $n=46$ organoids from 2 separate wells, UK-5099 $n=26$ organoids from 2 separate wells). (**g**) Images of organoids treated with IWP-2 and DAPT to promote differentiation with and without UK-5099. The blue arrowheads point to crypt domains and the yellow asterisks indicate autofluorescent lumens. (**h**) Organoid formation from crypts treated with the indicated single, double and triple drug combinations ($n=10$ experimental replicates, P values are for each treatment compared with wENR). (**i**) Transcript abundance in organoids showing the ratio of UK-5099-treated to control ($n=3$ experimental replicates, P values calculated for each transcript compared with wENR). (**j**) Heat map for additional transcripts from **i**. (**k**) Probability of cells infected with virus containing empty vector or both MPC1-iRFP and MPC2-mCherry also being GFP-positive ($n=4$ independent organoids with at least 15 infected cells counted). Data are mean ± s.e.m. $^{*}P<0.05$, $^{**}P<0.01$, $^{***}P<0.001$; NS, not significant. Scale bars, 50 μm (**a**) and 100 μm (**f**,**g**). P values for 6 h were calculated by one-way ANOVA with correction for multiple comparisons. All other P values were calculated using Student's t-test.

GSK-3beta inhibition. Given the previous suggestion that valproic acid might inhibit the MPC[33,34], we examined ^{13}C-glucose flux with and without valproic acid and found that valproic acid had no effect on the kinetics of citrate labelling, demonstrating that, at the concentrations used, this drug does not inhibit MPC activity (Supplementary Fig. 6a).

These observations of enhanced stem cell function and previously described metabolic effects (Fig. 5d–f) of UK-5099 treatment were

accompanied by changes in the expression of molecular markers of stemness. UK-5099 treatment in mixed organoid populations led to a robust increase in several stem cell markers, including *Lgr5*, *Ascl2*, *Cd44* and *Myc*, along with a substantial decrease in the abundance of the *Krt20*, *Villin1*, *Chga* and *Fabp2* differentiation markers (Fig. 6i,j and Supplementary Table 4). These data demonstrate that loss of mitochondrial pyruvate import leads to enhanced maintenance of molecular and functional markers of ISCs (and decreased markers of differentiation) to a degree similar to well-described stem-cell-maintaining agents.

Finally, we performed the converse of prior experiments and tested the hypothesis that forced expression of *Mpc1* and *Mpc2* in LGR5$^+$ ISCs causes a loss of stemness. Indeed, using a previously validated system for overexpression[14], we found that those cells expressing exogenous *Mpc1* and *Mpc2*, which are both required for MPC function, were much less likely to maintain *Lgr5* expression, as indicated by EGFP fluorescence (Fig. 6k and Supplementary Fig. 6b and Supplementary Table 7). This is consistent with work suggesting that stimulating glucose oxidation with the small molecule dichloroacetate (DCA) or by substitution of glucose with galactose promotes differentiation[10].

DISCUSSION

Our studies in *Drosophila*, intestinal organoids and mice provide strong evidence that the MPC is necessary and sufficient in a cell autonomous manner to suppress stem cell proliferation. Consistent with this, we have demonstrated that ISCs maintain low expression of the subunits that comprise the MPC, which enforces a mode of carbohydrate metabolism wherein glucose is metabolized in the cytosol to pyruvate and other biosynthetic intermediates. This glycolytic metabolic program appears to be sufficient to drive robust and continuous stem cell proliferation[35]. We also observed high mitochondrial content in ISCs, which must be geared primarily toward biosynthetic functions and/or oxidation of other substrates such as fatty acids. Increased fatty acids, the metabolism of which is enhanced in MPC-deficient and MPC-inhibited organoids, have been shown to promote ISC expansion and proliferation via enhanced beta-catenin signalling and increasing tumour-initiating capacity[36]. MPC expression increases following differentiation, consistent with the shift in demand from macromolecule biosynthesis to ATP production in support of post-mitotic differentiated cell function. A similar switch in MPC expression can be seen following differentiation of embryonic stem cells, haematopoietic stem cells and trophoblast stem cells[37–41]. Conversely, MPC expression is reduced after reprogramming fibroblasts to induced pluripotent stem cells[42–45]. This suggests that the effects of altering pyruvate flux that we observe herein might not be restricted to ISCs, but instead be representative of similar effects on multiple stem cell populations (see also the accompanying manuscript on hair follicle stem cells[46]). Interestingly, Myc is known to drive a metabolic program that is similar to that observed following MPC loss, characterized by increased glycolysis and reliance on glutamine and fatty acid oxidation with reduced glucose oxidation[47–49]. This suggests that Myc may play a role in repressing the MPC in stem cells, possibly acting downstream of Wnt/beta-catenin signalling[50]. Consistent with this, Myc and its repressive co-factors localize to the *Mpc1* promoter and *Myc* expression is strongly anti-correlated with *Mpc1* expression (Supplementary Fig. 6c)[14,51–54].

Taken together, our studies demonstrate that changes in the MPC and mitochondrial pyruvate metabolism are required to properly orchestrate the proliferation and homeostasis of intestinal stem cells. Importantly, this metabolic program—mediated at least partially by the MPC—appears to be instructive for, rather than a downstream consequence of, cell fate. Future work will define the extent to which the results presented herein relate to those showing that diet quality and quantity can modulate ISC behaviour. It is tempting to speculate that ISC metabolism is used as a signal for increased or decreased demand for intestinal epithelium. Perhaps of most importance will be to define the mechanisms whereby altered partitioning of pyruvate metabolism affects stem cell proliferation and fate. We speculate that the robust changes that we observed in fatty acid oxidation and histone acetylation, which are probably downstream of altered metabolite utilization for acetyl-CoA production, play an important role[36,55–57]. While the mechanisms are not as yet defined, these studies establish a paradigm wherein mitochondrial metabolism does not merely provide a permissive context for proliferation or differentiation, but rather plays a direct and instructive role in controlling stem cell fate. □

METHODS

Methods, including statements of data availability and any associated accession codes and references, are available in the online version of this paper.

Note: Supplementary Information is available in the online version of the paper

ACKNOWLEDGEMENTS

We thank B. Edgar (University of Utah, USA) for stocks and reagents, C. Micchelli (Washington University School of Medicine, USA) for providing the *Notch* RNAi line, K. Beebe for helpful advice and comments on the *Drosophila* intestinal studies, G. Lam for establishing the *Drosophila* MPC overexpression strain, O. Yilmaz and D. Sabatini for assistance and insight into intestinal stem cell metabolism, D. Tantin for critiques and comments, members of the Rutter laboratory for assistance and advice, J. O'Shea, R. Orbus and C. DeHeer for assistance with NanoString, W. Swiatek for mouse assistance, ARUP Institute for Clinical and Experimental Pathology, and S. R. Tripp and E. Hammond for histology; L. Nikolova at the University of Utah Electron Microscopy Core Laboratory performed electron microscopy; mass spectrometry analysis was performed at the Mass Spectrometry and Proteomics Core Facility at the University of Utah. Mass spectrometry equipment was obtained through NCRR Shared Instrumentation Grant no. 1 S10 RR020883-01, 1 S10 RR025532-01A1, NIH 1 S10OD021505-01 (J.E.C.) and the Diabetes and Metabolism Center at the University of Utah. This study was conducted with support from the Biorepository and Molecular Pathology Shared Resource supported by the Cancer Center Support Grant awarded to the Huntsman Cancer Institute by the National Cancer Institute of the National Institutes of Health. Nanostring transcript analysis utilized the Molecular Diagnostics Section of the Biorepository and Molecular Pathology Shared Resource and was supported by the National Cancer Institute of the National Institutes of Health under Award Number P30CA042014 (the content is solely the responsibility of the authors and does not necessarily represent the official views of the NIH). J. Marvin at the University of Utah Flow Cytometry Facility carried out flow sorting (National Cancer Institute through Award Number 5P30CA042014-24, National Center for Research Resources of the National Institutes of Health under Award Number 1S10RR026802-01). Funding was also provided by HHMI (J.R.), Treadwell (J.R.) and RO1GM094232 (to J.R. and C.S.T.). J.C.S. was supported by an NIH Developmental Biology Training Grant (5T32 HD07491) and a University of Utah Graduate Research Fellowship. D.R.W. was supported by a University of Utah Graduate Research Fellowship.

AUTHOR CONTRIBUTIONS

Conceptualization, J.C.S., D.R.W., C.S.T. and J.R.; methodology, J.C.S., D.R.W., C.B., H.Z., P.W., J.T., A.F., J.M., L.K.S., C.S.E., K.A.O., D.D., P.K., M.P.B., D.Y.L., J.E.C., H.R.C., W.E.L., C.S.T. and J.R.; investigation, J.C.S., D.R.W., C.B., H.Z., P.W., J.T., A.F., J.M., L.K.S., C.S.E., R.M., D.D. and P.K.; formal analysis, J.C.S., D.R.W., C.B., P.W., T.C.W., R.M., L.J., R.J.D. and J.E.C.; writing—original draft, review and editing,

J.C.S., D.R.W., C.S.T. and J.R.; funding acquisition, C.S.T. and J.R.; resources, D.Y.L., J.C., C.S.T. and J.R.; supervision, C.S.T. and J.R.

COMPETING FINANCIAL INTERESTS

The authors declare no competing financial interests.

Published online at http://dx.doi.org/10.1038/ncb3593

1. Warburg, O. On respiratory impairment in cancer cells. *Science* **124,** 269–270 (1956).
2. Birsoy, K. *et al.* An essential role of the mitochondrial electron transport chain in cell proliferation is to enable aspartate synthesis. *Cell* **162,** 540–551 (2015).
3. Sullivan, L. B. *et al.* Supporting aspartate biosynthesis is an essential function of respiration in proliferating cells. *Cell* **162,** 552–563 (2015).
4. Flavell, R. B. Mitochondrion as a multifunctional organelle. *Nature* **230,** 504–506 (1971).
5. Martínez-Reyes, I. *et al.* TCA cycle and mitochondrial membrane potential are necessary for diverse biological functions. *Mol. Cell* **61,** 199–209 (2016).
6. Simsek, T. *et al.* The distinct metabolic profile of hematopoietic stem cells reflects their location in a hypoxic niche. *Cell Stem Cell* **7,** 380–390 (2010).
7. Ito, K. & Suda, T. Metabolic requirements for the maintenance of self-renewing stem cells. *Nat. Rev. Mol. Cell Biol.* **15,** 243–256 (2014).
8. Stringari, C. *et al.* Metabolic trajectory of cellular differentiation in small intestine by Phasor Fluorescence Lifetime Microscopy of NADH. *Sci. Rep.* **2,** 568 (2012).
9. Fan, Y.-Y. *et al.* A bioassay to measure energy metabolism in mouse colonic crypts, organoids, and sorted stem cells. *Am. J. Physiol. Gastrointest. Liver Physiol.* **309,** G1–G9 (2015).
10. Rodríguez-Colman, M. J. *et al.* Interplay between metabolic identities in the intestinal crypt supports stem cell function. *Nature* **543,** 424–427 (2017).
11. Berger, E. *et al.* Mitochondrial function controls intestinal epithelial stemness and proliferation. *Nat. Commun.* **7,** 13171 (2016).
12. Bricker, D. K. *et al.* A mitochondrial pyruvate carrier required for pyruvate uptake in yeast, *Drosophila*, and humans. *Science* **337,** 96–100 (2012).
13. Herzig, S. *et al.* Identification and functional expression of the mitochondrial pyruvate carrier. *Science* **337,** 93–96 (2012).
14. Schell, J. C. *et al.* A role for the mitochondrial pyruvate carrier as a repressor of the Warburg effect and colon cancer cell growth. *Mol. Cell* **56,** 400–413 (2014).
15. Sato, T. *et al.* Single Lgr5 stem cells build crypt-villus structures *in vitro* without a mesenchymal niche. *Nature* **459,** 262–265 (2009).
16. Sato, T. & Clevers, H. Primary mouse small intestinal epithelial cell cultures. *Methods Mol. Biol.* **945,** 319–328 (2013).
17. Uhlen, M. *et al.* Towards a knowledge-based Human Protein Atlas. *Nat. Biotechnol.* **28,** 1248–1250 (2010).
18. Uhlen, M., Pontén, F. & Lindskog, C. Charting the human proteome: understanding disease using a tissue-based atlas. *Science* **347,** 1274–1274 (2015).
19. Jiang, H. & Edgar, B. A. Intestinal stem cell function in *Drosophila* and mice. *Curr. Opin. Genet. Dev.* **22,** 354–360 (2012).
20. Li, H. & Jasper, H. Gastrointestinal stem cells in health and disease: from flies to humans. *Dis. Model Mech.* **9,** 487–499 (2016).
21. Dutta, D. *et al.* Regional cell-specific transcriptome mapping reveals regulatory complexity in the adult *Drosophila* midgut. *Cell Rep.* **12,** 346–358 (2015).
22. Buchon, N. *et al.* Morphological and molecular characterization of adult midgut compartmentalization in *Drosophila*. *Cell Rep.* **3,** 1725–1738 (2013).
23. Wu, J. S. & Luo, L. A protocol for mosaic analysis with a repressible cell marker (MARCM) in *Drosophila*. *Nat. Protoc.* **1,** 2583–2589 (2006).
24. Micchelli, C. A. & Perrimon, N. Evidence that stem cells reside in the adult *Drosophila* midgut epithelium. *Nature* **439,** 475–479 (2006).
25. Ohlstein, B. & Spradling, A. The adult *Drosophila* posterior midgut is maintained by pluripotent stem cells. *Nature* **439,** 470–474 (2006).
26. Li, H. *et al.* *Drosophila* larvae synthesize the putative oncometabolite L-2-hydroxyglutarate during normal developmental growth. *Proc. Natl Acad. Sci. USA* **114,** 1353–1358 (2017).
27. Micchelli, C. A. Whole-mount immunostaining of the adult *Drosophila* gastro-intestinal tract. *Methods* **68,** 273–279 (2014).
28. Vigueira, P. A. *et al.* Mitochondrial pyruvate carrier 2 hypomorphism in mice leads to defects in glucose-stimulated insulin secretion. *Cell Rep.* **7,** 2042–2053 (2014).
29. Vacanti, N. M. *et al.* Regulation of substrate utilization by the mitochondrial pyruvate carrier. *Mol. Cell* **56,** 425–435 (2014).
30. Bender, T., Pena, G. & Martinou, J.-C. Regulation of mitochondrial pyruvate uptake by alternative pyruvate carrier complexes. *EMBO J.* **34,** 911–924 (2015).
31. Yang, C. *et al.* Glutamine oxidation maintains the TCA cycle and cell survival during impaired mitochondrial pyruvate transport. *Mol. Cell* **56,** 414–424 (2014).
32. Yin, X. *et al.* Niche-independent high-purity cultures of Lgr5+ intestinal stem cells and their progeny. *Nat. Methods* **11,** 106–112 (2014).
33. Aires, C. C. P. *et al.* Pyruvate uptake is inhibited by valproic acid and metabolites in mitochondrial membranes. *FEBS Lett.* **582,** 3359–3366 (2008).
34. Benavides, J., Martin, A., Ugarte, M. & Valdivieso, F. Inhibition by valproic acid of pyruvate uptake by brain mitochondria. *Biochem. Pharmacol.* **31,** 1633–1636 (1982).
35. Dailey, M. J. Nutrient-induced intestinal adaption and its effect in obesity. *Physiol. Behav.* **136,** 74–78 (2014).
36. Beyaz, S. *et al.* High-fat diet enhances stemness and tumorigenicity of intestinal progenitors. *Nature* **531,** 53–58 (2016).
37. Cao, F. *et al.* Transcriptional and functional profiling of human embryonic stem cell-derived cardiomyocytes. *PLoS ONE* **3,** e3474 (2008).
38. Chen, B.-Z. *et al.* Identification of microRNAs expressed highly in pancreatic islet-like cell clusters differentiated from human embryonic stem cells. *Cell Biol. Int.* **35,** 29–37 (2011).
39. Ralston, A. *et al.* Gata3 regulates trophoblast development downstream of Tead4 and in parallel to Cdx2. *Development* **137,** 395–403 (2010).
40. Muntean, A. G. *et al.* The PAF complex synergizes with MLL fusion proteins at HOX loci to promote leukemogenesis. *Cancer Cell* **17,** 609–621 (2010).
41. Keller, M. A. *et al.* Transcriptional regulatory network analysis of developing human erythroid progenitors reveals patterns of coregulation and potential transcriptional regulators. *Physiol. Genomics* **28,** 114–128 (2006).
42. Tateno, H. *et al.* Glycome diagnosis of human induced pluripotent stem cells using lectin microarray. *J. Biol. Chem.* **286,** 20345–20353 (2011).
43. Nishino, K. *et al.* DNA methylation dynamics in human induced pluripotent stem cells over time. *PLoS Genet.* **7,** e1002085 (2011).
44. Saito, S. *et al.* Possible linkages between the inner and outer cellular states of human induced pluripotent stem cells. *BMC Syst. Biol.* **5** (Suppl. 1), S17 (2011).
45. Wang, X.-M. *et al.* The gene expression profiles of induced pluripotent stem cells from individuals with childhood cerebral adrenoleukodystrophy are consistent with proposed mechanisms of pathogenesis. *Stem Cell Res. Ther.* **3,** 39 (2012).
46. Flores, A. *et al.* Lactate dehydrogenase activity drives hair follicle stem cell activation. *Nat. Cell Biol.* http://dx.doi.org/10.1038/ncb3575 (2017).
47. Camarda, R. *et al.* Inhibition of fatty acid oxidation as a therapy for MYC-overexpressing triple-negative breast cancer. *Nat. Med.* **22,** 427–432 (2016).
48. Boroughs, L. K. & DeBerardinis, R. J. Metabolic pathways promoting cancer cell survival and growth. *Nat. Cell Biol.* **17,** 351–359 (2015).
49. Edmunds, L. R. *et al.* c-Myc programs fatty acid metabolism and dictates acetyl-CoA abundance and fate. *J. Biol. Chem.* **289,** 25382–25392 (2014).
50. Pate, K. T. *et al.* Wnt signaling directs a metabolic program of glycolysis and angiogenesis in colon cancer. *EMBO J.* **33,** 1454–1473 (2014).
51. Gerstein, M. B. *et al.* Architecture of the human regulatory network derived from ENCODE data. *Nature* **489,** 91–100 (2012).
52. Wang, J. *et al.* Factorbook.org: a Wiki-based database for transcription factor-binding data generated by the ENCODE consortium. *Nucleic Acids Res.* **41,** D171–D176 (2013).
53. Wang, J. *et al.* Sequence features and chromatin structure around the genomic regions bound by 119 human transcription factors. *Genome Res.* **22,** 1798–1812 (2012).
54. Karolchik, D. *et al.* The UCSC Genome Browser database: 2014 update. *Nucleic Acids Res.* **42,** D764–D770 (2014).
55. McCool, K. W., Xu, X., Singer, D. B., Murdoch, F. E. & Fritsch, M. K. The role of histone acetylation in regulating early gene expression patterns during early embryonic stem cell differentiation. *J. Biol. Chem.* **282,** 6696–6706 (2007).
56. Roostaee, A., Benoit, Y. D., Boudjadi, S. & Beaulieu, J.-F. Epigenetics in intestinal epithelial cell renewal. *J. Cell. Physiol.* **231,** 2361–2367 (2016).
57. Golob, J. L., Paige, S. L., Muskheli, V., Pabon, L. & Murry, C. E. Chromatin remodeling during mouse and human embryonic stem cell differentiation. *Dev. Dyn.* **237,** 1389–1398 (2008).

METHODS

Mice. Heterozygous *Lgr5*-EGFP-IRES-CreERT2 mice were obtained from Jackson Labs[58]. *MPC1* fl/fl mice were generated as previously described[59]. Control animals consisted of *Lgr5*-EGFP-IRES-CreERT2 × *MPC1* WT/WT or *MPC1* fl/fl mice negative for *Lgr5*-EGFP-IRES-CreERT2. For *in vivo* knockout 6- to 8-week-old mice were injected intraperitoneally with 100 µl of 20 mg ml^{-1} tamoxifen (Sigma Aldrich T5648) dissolved in peanut oil (Sigma Aldrich P2144) for three successive days and euthanized 8, 30 or 160 days later. BrdU (Invitrogen b23151) was dissolved in PBS to 10 mg ml^{-1} and 100 µl was injected intraperitoneally 4 h before euthanization to label dividing cells. Injections were carried out in the morning (between 7:00 and 11:00) and tissue was collected 4 h later ±10 min from the time of injection. A 2 cm section was used for crypt dissociation and organoid formation as described below. The remainder of the small intestine was divided and fixed in buffered 10% formalin (Fisher Scientific 23-245-685) as previously described[60] for 48 h, transferred to 70% ethanol and paraffin-embedded for sectioning and staining. No formal randomization was performed for animal studies, animals were used as they became available, paired with littermate controls where possible, there was no preference for male or female animals, and both genders were included in each analysis. All IACUC guidelines were followed and the protocol for animal experiments carried out in this study was submitted to the University of Utah Institutional Animal Care and Use Committee.

***Drosophila* stocks.** *Drosophila* stocks were maintained on standard food containing 3% sucrose, 6% glucose, 8% yeast and 1% agar in a 25 °C incubator. For dMPC1 genetic studies, control flies were homozygous for a precise excision of the *P(XP)CG14290[d00809]* P-element insertion, and mutant flies were *trans*-heterozygous for the two deletion alleles, *dMPC1*[1] and *dMPC1*[2], as described previously[12]. *Dl-GAL4* (a gift from B. Edgar) was used to target RNAi to the ISCs and *esg-GAL4* (a gift from B. Edgar) was used to target RNAi to the ISCs and enteroblasts. RNAi transgenic stocks are as follows: *UAS-dMPC1* RNAi and *UAS-dMPC2*-RNAi[12], *UAS-PDH-E1* (VDRC101856), *UAS-PDH-E2* (VDRC 102893) and *UAS-Notch*-RNAi (a gift from C. Micchelli). Temperature-sensitive *Tub-GAL80ts* was utilized to restrict RNAi to adults. For temperature-shift experiments, animals were raised at 18 °C and 4–5-day-old adults were transferred to 29 °C for five days after which intestines were dissected for analysis. *Pseudomonas* infections were performed as described previously[27]. The *Pseudomonas* strain was a gift from B. Edgar. Overexpression of the *MPC* was achieved by inserting the open reading frames for *dMPC1* and *dMPC2* downstream from the UAS promoter in the *pUAST-attB* vector, with the coding sequence for the P2A peptide joining the two MPC coding regions[61]. This was inserted into the *attP40* site on the second chromosome using standard methods, and expression was achieved using GAL4 drivers specific to the ISCs or progenitor cells. All *Drosophila* studies were performed following standard ethical guidelines for working with this organism. As is standard in studies of *Drosophila* intestinal stem cells, all experiments were performed in females, which have a higher rate of basal stem cell proliferation than males. Experiments were conducted in adults aged four days to three weeks after eclosion.

Mosaic analysis. The MARCM system was used to generate wild-type and *dMPC1* mutant lineages as previously described[23]. Four- to five-day-old adult female flies of the following genotypes were subjected to two 38 °C heat pulses for 30–40 min: *y, w, hs-FLP, UAS-GFP / w ; +; Tub-GAL4, FRT82B, Tub-Gal80 / FRT82B* (control), *y, w, hs-FLP, UAS-GFP / w ; +; Tub-GAL4, FRT82B, Tub-Gal80 / FRT82B dMPC1*[1] (mutant). Clones were analysed three weeks after induction. The number of nuclei in GFP-expressing clones was used for quantification. For the *dMPC1* MARCM studies in the presence of *Notch* RNAi, intestines were analysed five days after clone induction. Intestines were stained with antibodies to detect GFP and Prospero, with DAPI to mark nuclei. Animals of the following genotype were used: *y, w, hs-FLP, UAS-GFP / w ; UAS-Notch-RNAi ; Tub-GAL4, FRT82B, Tub-GAL80 / FRT82B* (control, *Notch* RNAi only), *y, w, hs-FLP,UAS-GFP / w; UAS-Notch-RNAi; Tub-GAL4, FRT82B, Tub-GAL80 / FRT82B dMPC1*[1] (*Notch* RNAi and *dMPC1* mutant clones). Only clones that were negative for enteroendocrine cells (Prospero negative) and enterocytes (larger nuclei) were included in the analysis.

Histology and immunostaining. Adult flies were dissected in 1×PBS and the gastrointestinal tract was fixed in 4% formaldehyde (Polysciences, EM grade) overnight at 4 °C. Tissues were washed four times with 0.1% Triton, 1×PBS (PBST) and incubated with PBST and primary antibodies overnight, washed again, and then incubated for 3–4 h with secondary antibodies in PBST. Samples were mounted using Vectashield (Vector) with DAPI. Antibody information is provided in Supplementary Table 5. Images were acquired using an Olympus FV1000 confocal microscope and assembled into *Z* stack projections for the figures. For the RNAi experiments, GFP-positive cells were quantified per ×40 frame in the mid-R2 region of the intestine. For the number of dividing cells, the average number of PHH3-positive cells for the entire midgut was reported.

Crypt and single-cell isolation. Small intestinal crypts and single GFP-positive cells were isolated as previously described[15]. The entire small intestine was harvested, opened longitudinally and washed with PBS. Mucus and villi were scraped and discarded using a thin glass coverslip and tissue was cut into small (approximately 2 cm) sections. These were washed again in PBS and incubated in 2.5 mM EDTA diluted in PBS for 1 h with gentle agitation at 4 °C. Crypts were liberated and collected by centrifugation (400*g* for 5 min at 4 °C) followed by washing with PBS to remove EDTA. Crypts in PBS were passed through a 70-µm cell strainer and centrifuged as before. This pellet was resuspended in 50% culture medium (described below) and 50% Corning Growth Factor-Reduced Matrigel (Fisher Scientific no. 356231) for culture or dissociated for single cells. Single-cell isolation was carried out as described previously[62] by resuspending crypts in TrypLE Express (Invitrogen no. 1260413) with DNase I (Gold Biotechnology no. D-300-1) for 10 min at 37 °C. Dissociated cells were washed in culture medium without growth factors, centrifuged at 700*g*, resuspended and passed through a 35-µm strainer (Fisher Scientific no. 08-771-23) and analysed by FACS. Negative staining was carried out with DAPI and single live cells were collected, pelleted and snap-frozen for analysis or resuspended for culture.

Culture of crypts and single cells. Crypts or single cells were maintained as previously described[15] with minimal modification. For regional specific assays of organoid formation the intestine was divided up as follows: the duodenum was classified as the first 4–5 cm, jejunum was classified as the proximal half, and ileum the distal half. The entire colon, excluding the caecum and rectum were pooled and crypts isolated. Medium consisted of advanced DMEM/F12 (Invitrogen no. 12634028) medium prepared with HEPES (Invitrogen no. 15630-080), Glutamax (Invitrogen no. 35050061), and Penicillin–Streptomycin (Invitrogen no. 15140122) with N-2 supplement (Invitrogen no. 17502048), B27 serum-free supplement (Invitrogen no. 17504044) *N*-acetyl-L-cysteine (1 mM) containing all growth factors (Wnt3A to final concentration 2.5 ng ml^{-1}: Peprotech no. 315-20, Noggin to final concentration 100 ng ml^{-1}: Peprotech no. 250-38, EGF to final concentration 50 ng ml^{-1}: Gold Biotechnology no. 1350-04-500, mRSPO1-Fc-conditioned medium from 293T cells provided by C. Kuo at Stanford University, USA, as previously described[63]) and 50% Matrigel (Fisher Scientific no. 356321). Crypts were resuspended in medium and Matrigel was spotted in the centre of wells in a 48-well plate and allowed to polymerize at 37 °C prior to overlaying with medium. Inhibitors CHIR99021 (3 µM, R & D Systems no. 4423), valproic acid (1 mM made fresh each day, R & D Systems no. 28-151-100) and UK-5099 (10 µM, R & D Systems no. 4186) used to compare organoid formation from crypts were added to the crypt Matrigel mixture as well as to the medium overlay and changed every 2–3 days. These drug concentrations were identified as standard from previous studies (CHIR99021: 3 µM, valproic Acid: 1 mM, and UK-5099 10 µM) but were titrated for efficacy at dosages of 0.5×, 1.0×, 3.0× and 9.0×. Total organoid number and number of crypt domains per organoid were counted after 9 days. For single cells, CHIR99021 and valproic acid were added to maintain Lgr5 stem cells as previously described[32] along with Rho kinase inhibitor Y-27613 (10 µM Fisher Scientific no. 125410), Jagged-1 (1 µM AnaSpec, Inc no. AS-61298).

Organoid knockout. Single Lgr5-EGFP-positive cells from *MPC1* fl/fl × *Lgr5*-EGFP-IRES-CreERT2 were sorted and plated as above. Control genetically matched samples received dimethylsulfoxide and genetic recombination was induced using (*Z*)-4-hydroxytamoxifen (200 nM, Fisher Scientific no. 34-1210). Organoids grown from these were re-sorted for live EGFP-positive cells and plated as above or collected for mRNA analysis. Prior to use of knockout organoid culture in further experiments, loss of MPC1 was verified by western blot where we also looked for a significant destabilization of MPC2. If we could still detect MPC1 protein, cultures were retreated with (*Z*)-4-hydroxytamoxifen and purified by flow cytometry. In addition, we routinely assessed MPC1 when blotting for other targets to ensure the knockout was stable and no wild-type escaper cells repopulated the culture.

Secondary organoids. Organoids were passaged to single cells as above. Cell viability was determined by exclusion of 0.2% trypan blue (Sigma Aldrich) and both cell number and viability counted using the Cellometer Auto T4 (Nexcelom). Organoid formation and percentage of EGFP positivity from single live cells was measured once mature organoids had formed (7–9 days).

Organoid differentiation. Organoids grown for differentiation were passaged to single cells and allowed to establish for 6–8 days in standard medium. Following this, medium was replaced with medium lacking Wnt3A and RSPO1-conditioned medium (EN) lacking Wnt3A (ENR), or medium supplemented with 90 ng ml^{-1} Wnt3A (ENR +Wnt). Organoids were maintained in this medium for 48 h with fresh medium added after 24 h. To promote robust differentiation, IWP-2 (2 µM Fisher Scientific no. 35-331-0) and DAPT (10 µM Fisher Scientific no. 26-341-0) were added to organoid medium along with vehicle (dimethylsulfoxide) or UK-5099

DOI: 10.1038/ncb3593

(20 μM). Images were taken of live organoids to assess the loss of GFP signal. For passive differentiation, crypts were plated identically and allowed to form in wENR with CHIR and valproic acid. The medium was then changed to basal medium (wENR) treated with vehicle (dimethylsulfoxide) or UK-5099 (10 μM) and the emergence of hyperintense autofluorescent organoid lumens was observed and quantified.

MPC overexpression. Viral infection of Lgr5 stem cells was carried out as previously described with modifications[64]. Organoids were dissociated to single cells as described above with TrypLE and DNase followed by resuspension, filtering and pelleting. This cell pellet was then resuspended in 2× wENR that contained nicotinamide (10 mM), Y-27613 (10 μM), Polybrene (10 μg ml^{-1}) and CHIR99021 (3 μM). This cell suspension was added 1:1 with concentrated virus. The cell/virus mixture was incubated for 10 min at 37 °C, spun for 30 min at 200*g* at room temperature, resuspended and plated into 48-well plates and incubated in a tissue culture incubator for 4 h. After infection, cells were collected from wells, centrifuged at 700*g* for 10 min, washed and resuspended in fresh cold medium. This was mixed with Matrigel as described above and spotted for organoid growth. Lentivirus was produced as previously described[65]. *hMPC1* was subcloned into LeGO-iG2 from Addgene (no. 27341) with GFP substituted for iRFP713 from Addgene (no. 45468). *hMPC2* was subcloned into LeGO-iC2 from Addgene (no. 27345) (plasmid without *MPC2* also used as empty vector control). Lentiviral packaging and expression vectors were transfected into 293T with Lipofectamine 2000 (Invitrogen no. 11668019) to begin viral production. Supernatant was collected and pooled every 24 h from 24–96 h. This was then spun at 1,500*g* for 10 min to remove cell debris, passed through a 0.45 μm filter, and centrifuged in ∼30 ml aliquots overnight at 4 °C at 14,000*g* to concentrate viral particles. This was then resuspended in ∼500 μl HBSS and used for infection or aliquots and frozen at −80 °C. Organoids from single-cell infection were then allowed to form and imaged 6–8 days later for analysis.

Immunohistochemistry. All tissue processing, staining and analysis was done in a blinded manner. Paraffin sections (3–4 μm for immunohistochemistry, 7 μm for *in situ* hybridization) were cut on positively charged slides (BBC), placed at 60 °C for 30 min, and placed on an automated slide stainer (BenchMark, Discovery, Ventana Medical Systems) for processing. Slides were de-paraffinized with EZ prep solution, pre-treated with Cell Conditioner 1, pH 8.5, and stained with primary antibody for 1 h at 37 °C (Supplementary Table 5). Secondary antibody (rabbit 1:100 for VDAC1 and MPC1, rat 1:100 for BrdU) was applied and detection performed using IView DAB detection kit followed by haematoxylin counterstaining. Slides were scanned using an automated slide scanner (Zeiss Axio Scan.Z1). For analysis of Olfm4 and Lgr5 staining, images of Swiss-rolled proximal small intestine were used. Areas with a high density of crypts in cross-section that were continuous with villi were used for counting the number of stained cells. Multiple crypts from at least three different areas were counted and the average cell number was calculated per mouse. At least nine control and nine knockout animals were used and images were unused only if staining did not work or tissue orientation in cross-section was inadequate for counting. For histological analysis all small intestinal tissue was processed, stained and imaged blinded. Animals were excluded from analysis if tissue orientation, staining or acquisition failed and precluded analysis and for no other reason. For analysis, images of the proximal small intestine were selected that contained areas with crypts in cross-section continuous with villi. Three separate areas and a minimum of ten total crypts were analysed and averaged to give a value for that animal used for statistics. IRB for histology of human intestine: U of UT IRB 91019.

Immunofluorescence staining of mouse small intestine. Tissue for immunofluorescence was prepared as follows: the jejunum from LGR5 Cre^{+} mice was extracted and fixed at room temperature in 4% PFA for 2.5 h. This was followed by washing in PBS and equilibrating in OCT on ice then transferred to a chilled mould that was frozen on dry ice and stored at −80 °C. From this block, 10 μm sections were cut and transferred to slides, which were cured for 30 min at room temperature in the dark. OCT mounting media was washed twice, 5 min each using PBS at 37 °C. Sections were blocked/permeablized by treating for 1 h in a humid dark box in 1×PBS+Ca+Mg, 0.1% saponin, 10% donkey serum, 3% BSA. For staining: anti-MPC1 Sigma cat. no. HPA045119 in 1×PBS + 10% normal donkey serum,+3% BSA–no saponin at 1:100, incubated in the dark overnight at 4 °C. The next morning, slides were washed twice with PBS for 2 min each. Secondary antibody (1:100 (10 μg ml^{-1} donkey anti-rabbit IgG Alexa 594 conjugate) +5 μg ml^{-1} DAPI in 1 × PBS +3% BSA) was incubated at room temperature for 3 h. Slides were then washed twice with PBS as above and mounted using 100 mg ml^{-1} PVP mounting medium (Tris buffer +0.02% azide + 5% DABCO + 100 mg ml^{-1} polyvinylpyrrolidone + 1/25 volume glycerol) and cured for 2 h at room temperature.

Human colon crypt isolation and growth. Human colon biopsy samples for organoid cultures were collected under IRB 00051140, Molecular markers of sporadic hyperplastic colon polyps. Patients with a history of inflammatory bowel disease or patients with a personal or family history of familial colon cancer were excluded from the study. Briefly, study patients underwent screening colonoscopy as part of their regular clinical care. Participants scheduled for colonoscopy were not recruited for the study alone. Informed consent was obtained prior to any sedation. The study was approved by the IRB at the University of Utah and VA Medical Center. All samples were labelled with code numbers to protect confidentiality. All procedures were clinically indicated and recommended by the patients' physician or consultant. As per US preventative services task force (USPSTF), colon cancer screening is recommended for subjects who are 50 years and older for detection and management of colon polyps and colon cancer.

Removing colon polyps and obtaining colonic tissue is a standard procedure during colonoscopy. The biopsy forceps used to obtain colon biopsies are 2 to 3 mm in diameter. Endoscopic biopsies are commonly taken as part of regular clinical care to diagnose problems and evaluate suspicious tissues. The risks associated with this are minor; patients do not feel the biopsies because the colon does not have pain receptors (just stretch receptors), and bleeding is self-limited. In all situations, minimizing any potential risk to the participants was a priority. If in the clinical judgement of the physician, biopsies should not be taken, they are not. In addition, if taking biopsies will make the endoscopic procedure too long, they will not be taken.

Crypt imaging. Intestinal crypts were isolated as above and transferred to basal medium lacking growth factors. MitoTracker Red CMXRos (Invitrogen no. M7512) was prepared according to the manufacturer's instructions and added to suspended crypts in medium to a final concentration of 50 nM and incubated at 37 °C for 20 min.

Organoid imaging. Live organoids were imaged on the Axio Observer Z1 imaging system (Carl Zeiss) fitted with a heated humidity-controlled stage (LiveCell 05-11-0032 Rev B) and analysed using Zen 2 software (Carl Zeiss). The laser intensity was kept constant when making comparisons of organoids and adjustments for brightness and contrast were made to the entire image equally across groups being compared.

***In situ* hybridization.** For detection of *Lgr5* and *Olfm4* mRNA, we designed riboprobes targeting the coding sequence to the 3′UTR region of these genes (Supplementary Table 5). Targeted probe region DNAs were amplified using standard PCR, with the amplicon length of about 500 bp. These DNA amplicons were used to generate DIG-labelled riboprobes using T7 RNA polymerase. For staining, formalin-fixed paraffin-embedded tissue sections were de-paraffinized with Citrisolv, washed in 100% ethanol, and air-dried. Slides were blocked with Boehringer Blocking Reagent (Roche) and yeast tRNA at 68 °C for 1 h. Probes (0.5 ng ml^{-1}) were hybridized to sections at 68 °C overnight. After washing, sections were again blocked with Boehringer Blocking Reagent and 10% sheep serum at room temperature for 1 h. Alkaline-phosphatase-labelled sheep anti-DIG antibody (Roche) was incubated with sections at 1:2,000 dilution at 4 °C overnight. After washing, positive signals were developed using NBT/BCIP substrate (Thermo). Slides were then fixed in 10% neutral buffered formalin and mounted with aqueous mounting medium.

RNA extraction and analysis. Lgr5-GFP sorted cells were directly lysed in buffer RLT (Qiagen no. 79216) containing 2-mercaptoethanol (Sigma Aldrich no. M6250) and total lysate was assayed for transcript count as per the manufacturer's instructions. Total RNA was purified from organoids using the RNeasy Mini Kit (Qiagen) with 100 ng used for the assay.

mRNA analysis via NanoString. Transcript abundance was compared using the NanoString Elements platform. A custom gene set was created containing intestinal stem cell and differentiation genes including five housekeeping genes (*ActB*, *B2m*, *Cltc*, *GusB*, *Rpl19*, *Tbp* and *Ywhaz*). nSolver analysis software was used for data analysis with raw counts normalized to positive control probes and housekeeping genes. Only samples passing quality control were used for normalization and analysis. Data were visualized with Java Treeview and graphed using Prism 7 (GraphPad). Source data for the generation of heat maps in the manuscript are provided in Supplementary Tables 1–4. Sequences for probe design and source data for the generation of heat maps are provided in Supplementary Table 6.

Immunoblot analysis. Biological replicate organoids from independent single-cell isolations were harvested, washed in cold PBS and snap-frozen. Pellets were resuspended in tissue lysis buffer containing protease and phosphatase inhibitors as previously described[14]. Samples were disrupted by sonication, cleared by centrifugation at 10,000*g* for 5 min, and protein concentration was determined by BCA assay (Thermo Scientific) and diluted to allow for loading equal volumes. For histone acetylation assays, organoids were collected and nuclei were purified using

the NE-PER Nuclear and Cytoplasmic Extraction Kit (ThermoFisher cat. no. 78835) and following all instructions. Samples were resolved by SDS–PAGE, and analysed by immunoblotting for organoid experiments and Tris-Tricine Gel for *Drosophila* experiments. Primary antibodies were obtained from Abcam or Cell Signaling Technology: Supplementary Table 5. Corresponding secondary antibodies (rabbit: 680 and mouse: 800 channel) were visualized using the Odyssey scanner (Li-Cor).

Steady-state metabolomics. For steady-state metabolite accumulation, control and knockout organoids were passaged to single cells and replated in basal medium without drug (wENR). These organoids were grown for 8 days with medium changes every 2–3 days and approximately 12 h prior to harvest medium was refreshed. For harvest, organoids in Matrigel were mechanically disrupted and dissolved using ice-cold 0.9% sodium chloride, spun to 5,000*g* for 30 s, supernatant aspirated and samples snap-frozen with liquid nitrogen. Metabolites were extracted as previously described[12]. Briefly 450 µl of cold 90% methanol solution with internal standards (1 µg of d4-succinic acid) was added to each sample, vortexed briefly and sonicated for 3 min. This was kept at −20 °C for 1 h, centrifuged at 20,000*g* for 5 min at 4 °C, and the supernatant transferred to a new tube, and sample was dried in a speed-vac. All GC–MS analysis was performed with a Waters GCT Premier mass spectrometer fitted with an Agilent 6890 gas chromatograph and a Gerstel MPS2 autosampler. Dried samples were suspended in 40 µl of 40 mg ml^{-1} *O*-methoxylamine hydrochloride (MOX) in pyridine and incubated for one hour at 30 °C. Metabolites were identified and their peak area was recorded using QuanLynx. These data were transferred to an Excel spread sheet (Microsoft). Metabolite identity was established using a combination of an in-house metabolite library developed using pure purchased standards and the commercially available NIST library.

Flux metabolic labelling and cell lines. Organoids were passaged and grown as above. Multiple (∼30) 5 µl organoid Matrigel spots were plated into wells of a 6-well plate, overlaid with medium, and allowed to establish for approximately 1 week. Sixteen hours before beginning flux labelling, medium was changed to minimal medium (wENR as above) with and without UK-5099 (10 µM). At time 0, sample was taken for reference and medium was removed, organoid plates washed gently with warm PBS and changed to flux medium consisting of SILAC Advanced DMEM/F12 (ThermoFisher no. A2494301) with 10 mM U-$^{13}C_6$-glucose (CLM-1396-10), growth factors and supplements as above but lacking glutamine, unlabelled glucose, or amino acids. Flux labelling of cell lines was carried out as above in DMEM lacking any carbon source (Invitrogen 11966025) supplemented with 10 mM U-$^{13}C_6$-glucose (CLM-1396-10), Glutamax (Invitrogen no. 35050061), and 10% fetal calf serum. For drug treatment, 10 µM UK-5099 and 1 mM valproic acid were added to the above medium. C2C12 cells were purchased from ATCC (CRL-1772) and tMEFs were a gift from D. Tantin (University of Utah, USA). No cell lines used in this study were found in the database of commonly misidentified cell lines that is maintained by ICLAC and NCBI Biosample. The cell lines were not authenticated and were not tested for mycoplasma contamination.

Electron microscopy. Tissue was saved for electron microscopy by cutting approximately 1 mm doughnuts and fixed overnight at 4 °C in fresh 2.5% glutaraldehyde (Electron Microscopy Sciences no. 16320) diluted in PBS. The next day tissue was washed three times in cacodylate buffer. Secondary fixation was carried out in 2% osmium tetroxide at room temperature for 1 h followed by two washes with cacodylate buffer followed by one wash with water. Staining used saturated uranyl acetate for 1 h at room temperature, washed three times with water, and dehydrated with a graded ethanol series (30%, 50%, 70%, 95% ×2, 100% ×3, and finally absolute acetone). Infiltration was carried out with Epon epoxy resin (30% for 5 h, 70% overnight, 100% for 8 h with three changes) and tissue was embedded with 100% fresh resin. Polymerization in fresh resin was carried out at 60 °C for 48 h followed by ultracutting (Leica UC6 ultratome) at 70 nm. Images were collected using a JEM-1400 Plus Transmission Electron Microscope (JEOL).

Seahorse. Control and MPC1 knockout organoids for oxygen consumption studies were passaged by mechanical disruption rather than complete dissociation to single cells. Organoid fragments were spotted into a 6-well dish with multiple <10 µl spots per well and overlaid with 2 ml of organoid growth medium. Two days following plating, the medium was changed with the addition of vehicle or 10 µM UK-5099. For assay, seahorse analysis, organoids were extracted from Matrigel with gentle pipetting to minimize disaggregation. An XF96 well plate was coated with a 1:10 dilution of Matrigel in PBS and allowed to sit at room temperature for 1 h. Organoids were evenly seeded in each well with the respective medium (wENR CV ± UK-5099). The following day, organoids were run on an XF96e Analyzer for a Mito Stress Test in standard assay medium (DMEM, 25 mM glucose, 2 mM pyruvate, 2 mM glutamine, pH 7.4) using the manufacturer's protocol and standard drug concentrations (oligomycin 2 µM, FCCP 2 µM, rotenone 0.5 µM, and antimycin A 0.5 µM).

For fatty acid oxidation, substrate-limited medium was prepared as adapted from the stem cell recipe (all concentrations were kept the same except B27 supplement was 66.6 µl, D-glucose 0.5 mM, 1 mM glutamine and carnitine 0.5 mM per 5 ml of 4× medium). The following drugs were added to substrate-limited medium: 3 µM CHIR99021, 1 mM valproic acid, ±10 µM UK-5099. Medium was changed and the organoids were maintained for 6 h in substrate-limited conditions. FAO Assay running buffer was standard 1× KHB (111 mM NaCl, 4.7 mM KCl, 1.25 mM $CaCl_2$, 2.0 mM $MgSO_4$, 1.2 mM Na_2HPO_4) + 2.5 mM D-glucose, 0.5 mM L-carnitine, and 5 mM HEPES buffer (pH 7.4). The following drugs were added to 1× KHB: 3 µM CHIR99021, 1 mM valproic acid, ±10 µM UK-5099. Following medium change into 1× KHB, the plate was maintained at 37 °C in a non-CO_2 incubator. At 30 min post media change, 40 µM final Etomoxir (R & D Systems cat. no. 4539) or vehicle was added; and at 45 min post media change, BSA or palmitate, (Agilent cat. no. 102720-100) was added according to the manufacturer's protocol. Following the addition of the BSA or palmitate substrates, the assay was run in the XF96e Analyzer for the Mito Stress Test. The assay protocol was adapted as follows (three measurements per phase, acute injection followed by 3 min mixing, 3 min waiting, 3 min measuring) with the final concentrations of drugs as follows (oligomycin 2 µM, FCCP 2 µM, rotenone 0.5 µM and antimycin A 0.5 µM). Normalization to cellular protein was quantified by Pierce BCA assay (Fisher Scientific cat. no. 23227) and read on a photometric plate reader (Varioskan Flash). Results were analysed in WAVE software and processed through the XF Mito Stress Test Report and Glycolysis Stress Test Generators.

ENCODE ChIP-seq for MPC1 promoter. This track shows ChIP-seq data from the Myers Lab at the Hudson Alpha Institute for Biotechnology and by the laboratories of M. Snyder, M. Gerstein and S. Weissman at Yale University, P. Farnham at the University of Southern California, K. Struhl at Harvard, K. White at the University of Chicago, and V. Iyer at the University of Texas, Austin. These data were processed into uniform peak calls by the ENCODE Analysis Working Group pipeline developed by A. Kundaje. The clustering of the uniform peaks was performed by UCSC (https://genome.ucsc.edu/cgi-bin/hgGateway). The Factorbook motif identifications and localizations (and valuable assistance with interpretation) were provided by J. Wang, B. H. Kim and J. Zhuang of the Zlab (Weng Lab) at UMass Medical School.

Statistics and reproducibility. No pre-specified effect size was calculated, and no statistical method was used to predetermine sample size. For comparisons of multiple groups, an ordinary one-way ANOVA with Dunnett or Holm–Sidak correction for multiple comparisons (Fig. 1a groups compared with low, 1c groups compared with EN, 4f groups compared with wENR) was used. Statistical tests were appropriate for comparisons being made; for all *t*-tests and ANOVA, data meet assumptions of the tests; assessment of variation was carried out but not included. For mouse studies, an *n* of 10 was chosen for control (equal *Lgr5*-EGFP heterozygous × *Mpc1* WT/WT and *Lgr5*-EGFP wild-type × *Mpc1* fl/fl) and knockout (*Lgr5*-EGFP heterozygous × *Mpc1* fl/fl) comprised of both males and females. No statistical method was used to predetermine sample size. Experiments were not randomized. Investigators were not blinded to allocation during experiments and outcome assessment. Reproducibility: Fig. 2a: representative of two experiments; Fig. 2b: representative of two experiments; Fig. 2c representative of three experiments (pooled); Fig. 2d representative of three experiments; Fig. 2e representative of two experiments; Fig. 2f representative of two experiments; Fig. 2g representative of three experiments; Fig. 4a: representative of two experiments; Fig. 4b: representative of two experiments; Fig. 4c: representative of two experiments; Fig. 4d: representative of two experiments; Fig. 4g: representative of two experiments; Fig. 5d: representative of two experiments; Fig. 6a: representative of two experiments; Fig. 6b: representative of two experiments; Fig. 6c: representative of two experiments; Fig. 6d: representative of two experiments; Fig. 6e: four individual patients, $n = 6$ replicates, averaged and pooled; Fig. 6g: representative of two experiments; Fig. 6h: representative of two experiments; Fig. 6k: two independent infections, data pooled and Supplementary Fig. 2a: representative of three experiments; Supplementary Fig. 4b: representative of three experiments; Supplementary Fig. 6a: representative of two experiments and Supplementary Fig. 6b: two independent infections, data pooled (as in Fig. 6k).

Code availability. The software tools used for ENCODE are freely available at: https://genome.ucsc.edu/ENCODE/encodeTools.html.

Data availability. Previously published ENCODE ChIP-Seq data for Myc that were re-analysed here are available under UCSC accession codes wgEncodeEH000545, wgEncodeEH001867, wgEncodeEH000670, wgEncodeEH002800, wgEncodeEH000536 and wgEncodeEH001133.

Data corresponding to mRNA transcript abundance have been deposited at GEO under the accession numbers GSE100830 and GSE100831.

DOI: 10.1038/ncb3593

Metabolomics data have been deposited in Figshare and can be accessed under http://dx.doi.org/10.6084/m9.figshare.5117269.v1.

Source data for the figures have been provided as Supplementary Table 7.

All other data supporting the findings of this study are available from the corresponding author on reasonable request.

58. Barker, N. *et al.* Identification of stem cells in small intestine and colon by marker gene Lgr5. *Nature* **449,** 1003–1007 (2007).
59. Gray, L. R. *et al.* Hepatic mitochondrial pyruvate carrier 1 is required for efficient regulation of gluconeogenesis and whole-body glucose homeostasis. *Cell Metab.* **22,** 669–681 (2015).
60. Moolenbeek, C. & Ruitenberg, E. J. The 'Swiss roll': a simple technique for histological studies of the rodent intestine. *Lab. Anim.* **15,** 57–59 (1981).
61. Daniels, R. W., Rossano, A. J., Macleod, G. T. & Ganetzky, B. Expression of multiple transgenes from a single construct using viral 2A peptides in *Drosophila*. *PLoS ONE* **9,** e100637 (2014).
62. Sato, T. *et al.* Paneth cells constitute the niche for Lgr5 stem cells in intestinal crypts. *Nature* **469,** 415–418 (2011).
63. Ootani, A. *et al.* Sustained *in vitro* intestinal epithelial culture within a Wnt-dependent stem cell niche. *Nat. Med.* **15,** 701–706 (2009).
64. Simmini, S. *et al.* Transformation of intestinal stem cells into gastric stem cells on loss of transcription factor Cdx2. *Nat. Commun.* **5,** 5728 (2014).
65. Weber, K., Mock, U., Petrowitz, B., Bartsch, U. & Fehse, B. Lentiviral gene ontology (LeGO) vectors equipped with novel drug-selectable fluorescent proteins: new building blocks for cell marking and multi-gene analysis. *Gene Ther.* **17,** 511–520 (2010).

nature cell biology

DOI: 10.1038/ncb3593

In the format provided by the authors and unedited.

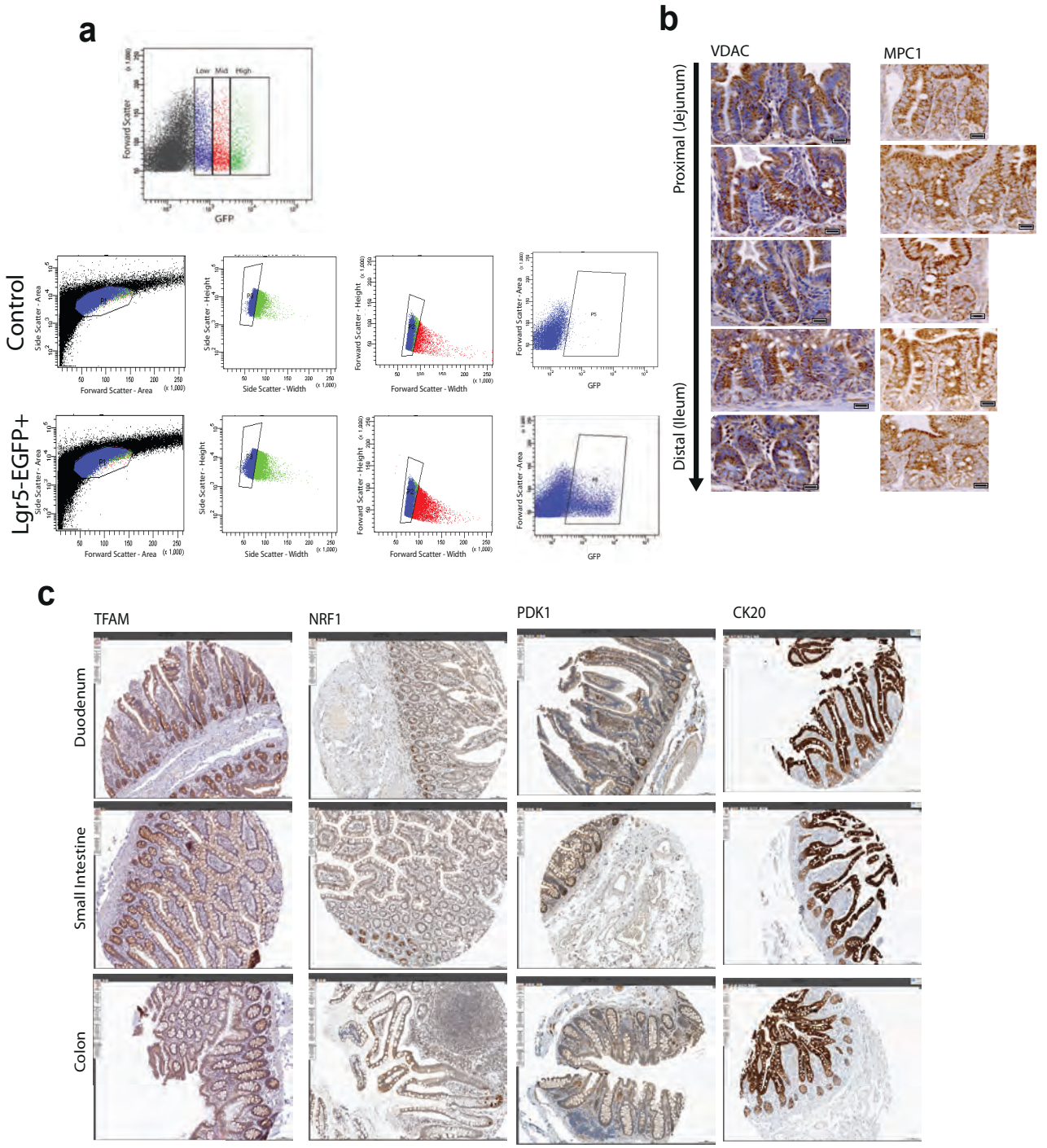

Supplementary Figure 1 Additional images of flow gating and IHC in mouse and human a, Gating startegy for sorting of Lgr5-EGFP positive stem cells for transcript abundance. Top showing final gating for collection of GFP-low, GFP-mid, and GFP-high cells for transcript abundance. Bottom showing full gating strategy exclusion of cell debris and purification of singlet cells. b, IHC of VDAC1 and MPC1 throughout the mouse small intestine from proximal to distal showing staining of crypt base and differentiating transient amplifying cells. (scale bar = 20 um). c, Human Protein Atlas (http://www.proteinatlas.org) images of duodenum, small intestine, and colon stained for TFAM, NRF1, PDK1, and CK20 (scale bar = 20 um (b), 100 um (c)).

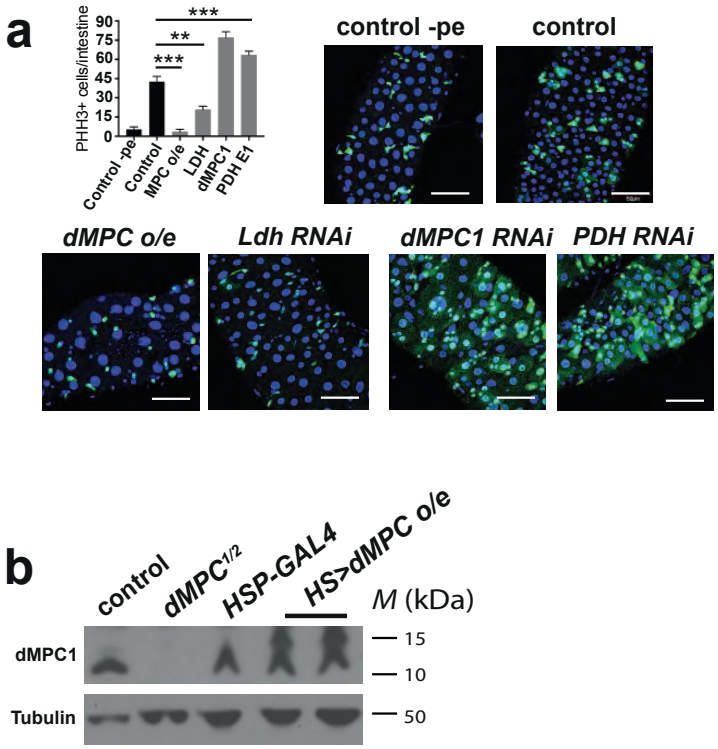

Supplementary Figure 2 Drosophila MPC regulates stem cell proliferation a, *esg-GAL4* used to target RNAi as indicated or MPC overexpression (o/e) under infected conditions (scale bar = 50 um). pHH3+ cells was quantified per intestine. (Control n=10 (no infection) Control (with infection) n=10, MPC O/E n=10, LDH RNAi n=10 MPC RNAi n= 10 PDH RNAi n=10) b, Western blot analysis to detect dMPC1 protein in control animals, *dMPC1* mutants, *HSP70-GAL4* controls, and *HSP70>UAS-dMPC1-dMPC2* transgenic animals following a 30-minute heat treatment and four hour recovery. Data are mean ± s.e.m. $*P < 0.05$, $**P < 0.01$, $***P < 0.001$. All *p* values were calculated using Student's *t*-test. Unprocessed western blots are provided in Supplementary Figure 7.

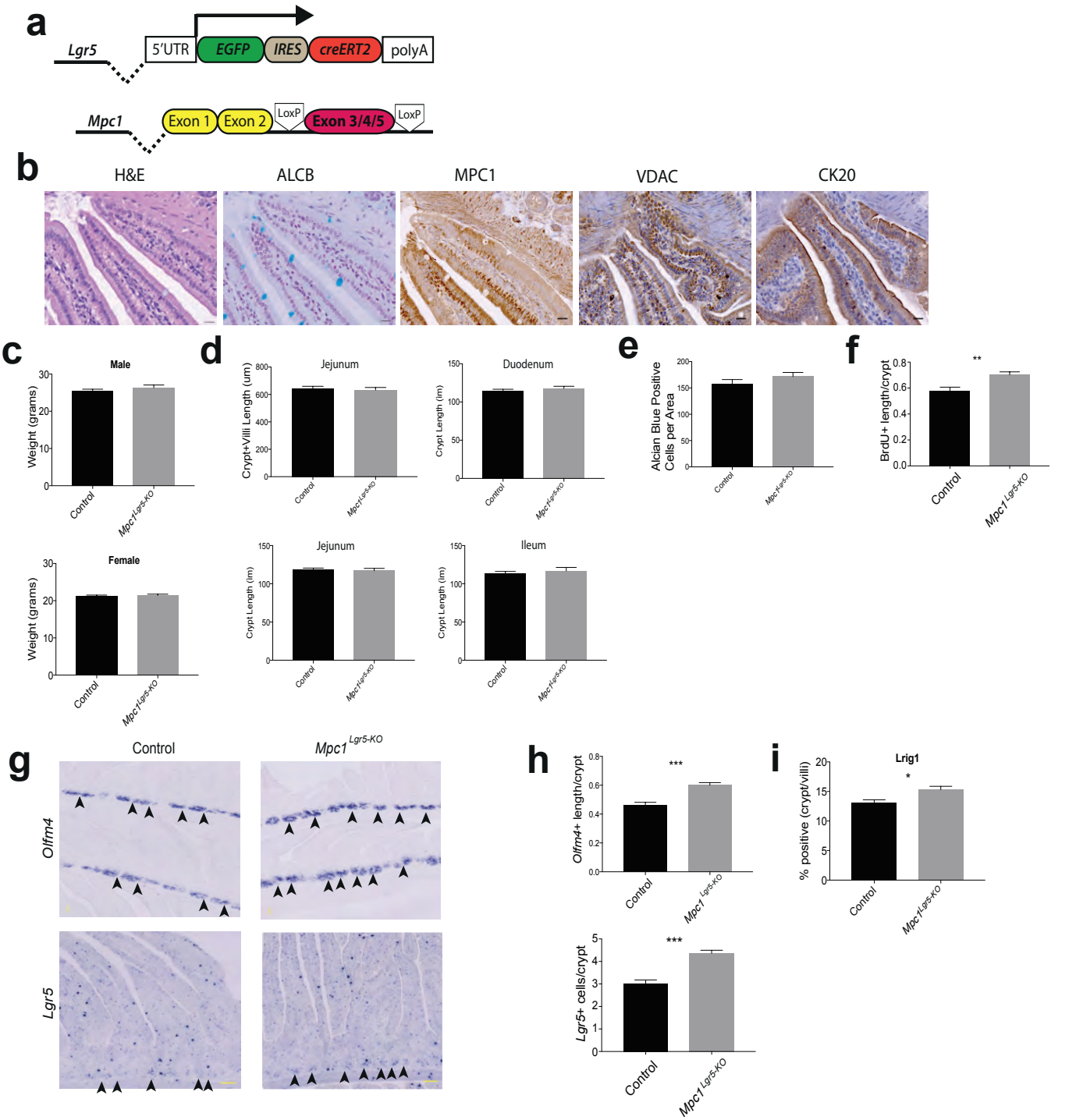

Supplementary Figure 3 MPC1 allele and additional quantification of in vivo phenotype a, Schematic of MPC1 allele used for inducible knockout. b, Close-up images of villi tip from MPC1 knockout stained for H&E, Alcian Blue, MPC1, VDAC and CK20 (scale bar = 20 um). c, Body weight for control and MPC1 knockout animals 30 days post-treatment. (n = 5 male control and knockout, n = 6 female control, = 3 knockout) d, Total crypt+villi height and crypt height from individual regions of the small intestine. (n = 9 control, = 10 knockout for crypt+villi, n = 10 control, = 9 knockout for crypt height from each region) e, Quantification of Alcian Blue positive cells per area of the proximal small intestine. (n = 10 control and knockout) f, Quantification fo BrdU positive cells per crypt of proximal small intestine. (n = 9 control, = 10 knockout) g, Images of Olfm4 and Lgr5 in situ in control and MPC1 knockout. (scale bar = 50 um) h, Additional quantification of in situ staining. (n = 9 control, n= 10 knockout) i, Quantification of Lrig1 IHC staining in control and MPC1 knockout proximal small intestine. (n = 9 control, n= 10 knockout) Data are mean ± s.e.m. $*P < 0.05$, $**P < 0.01$, $***P < 0.001$. All p values were calculated using Student's t-test.

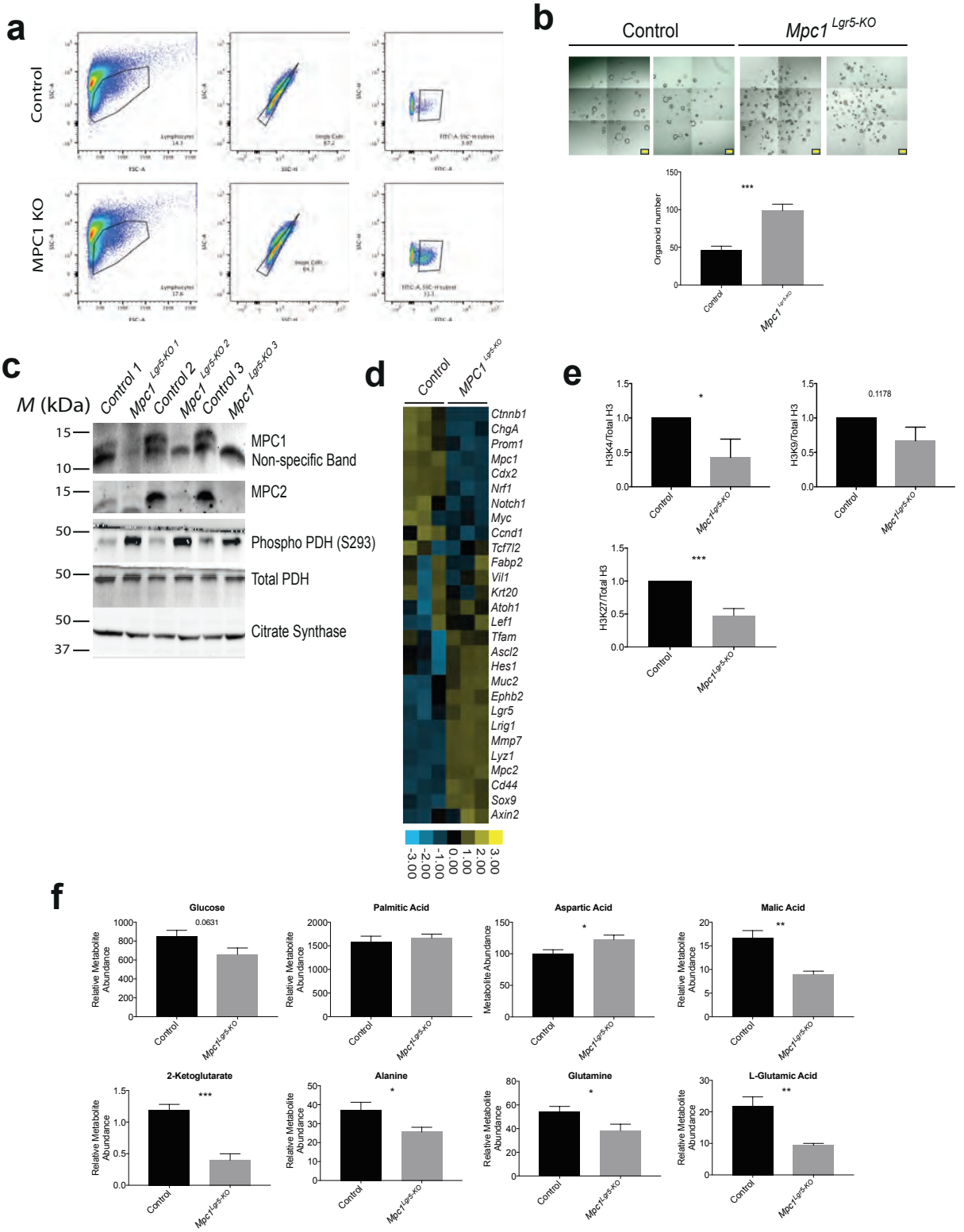

Supplementary Figure 4 Additional characterization of in vito Mpc1 Lgr5-KO a, Flow cytometry profile for organoids from control and MPC1 knockout cultures showing GFP positivity. b, Long-term cultures retain increased growth ability throughout extended passaging (over ~2 months) (n = 15 control and knockout, scale bar = 200 um) c, Control and MPC1 knockout organoid western blots for MPC1 and MPC2 and pyruvate dehydrogenase (phospho 293 and total). d, Transcript abundance of MPC1 knockout organoids showing stem and differentiation marks (n = 3). e, Quantification of specific Acetyl Histone H3 marks in control and knockout organoids (paired control set to 1.0) (n = 8 organoids). f, Steady state metabolite abundance for control and MPC1 knockout organoids (n = 6 control and knockout). Data are mean ± s.e.m. $*P < 0.05$, $**P < 0.01$, $***P < 0.001$. All p values were calculated using Student's t-test. Unprocessed western blots are provided in Supplementary Figure 7.

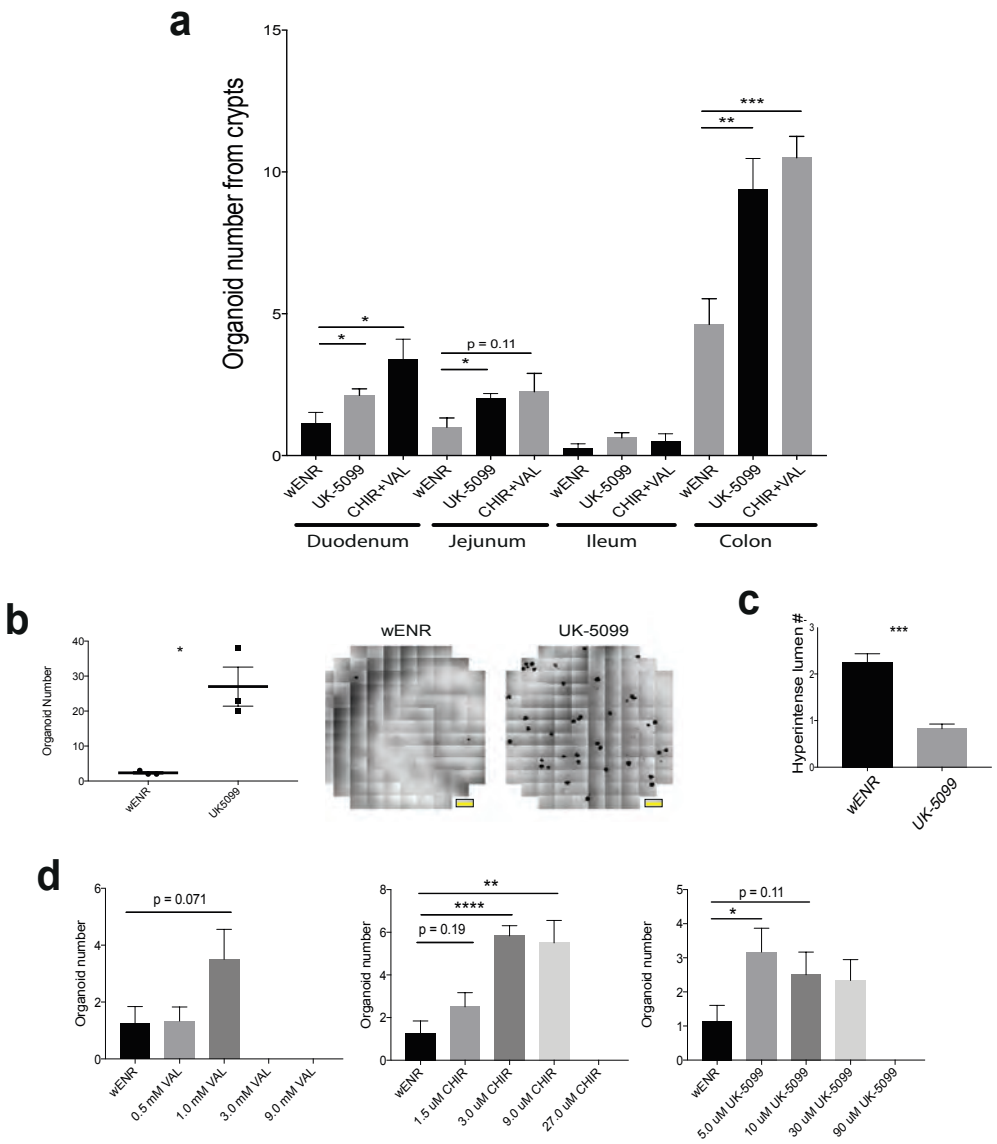

Supplementary Figure 5 Effects of UK-5099 in maintaining organoids. a, Organoid formation from different regions of small intestine and colon with treatment conditions (n = 6 per condition, p values by t-test with respect to wENR for each location). b, Loss of passaging efficiency in crypts maintained in wENR compared to UK-5099. When identical cell numbers are passaged normally, wENR treated are more likely to fail to passage. Images are of multiple matrigel/organoid spots of identical size (5uL) on a 6 well plate tiled to make one image (organoids from n = 3 wells were counted and number per well used for quantification, scale bar = 2000 um). c, Formation of hyperintense lumens in crypt organoids grown in wENR compared to UK-5099 3 days after changing media to remove CHIR99021 and Valproic acid (n = 69 total organoids from 6 individual wells). d, Dose curves for individual drugs in supporting organoid formation from crypts (n = 8 wENR, all other conditions n = 6, p value by t-test with respect to wENR). Data are mean ± s.e.m. $*P < 0.05$, $**P < 0.01$, $***P < 0.001$. All *p* values were calculated using Student's *t*-test.

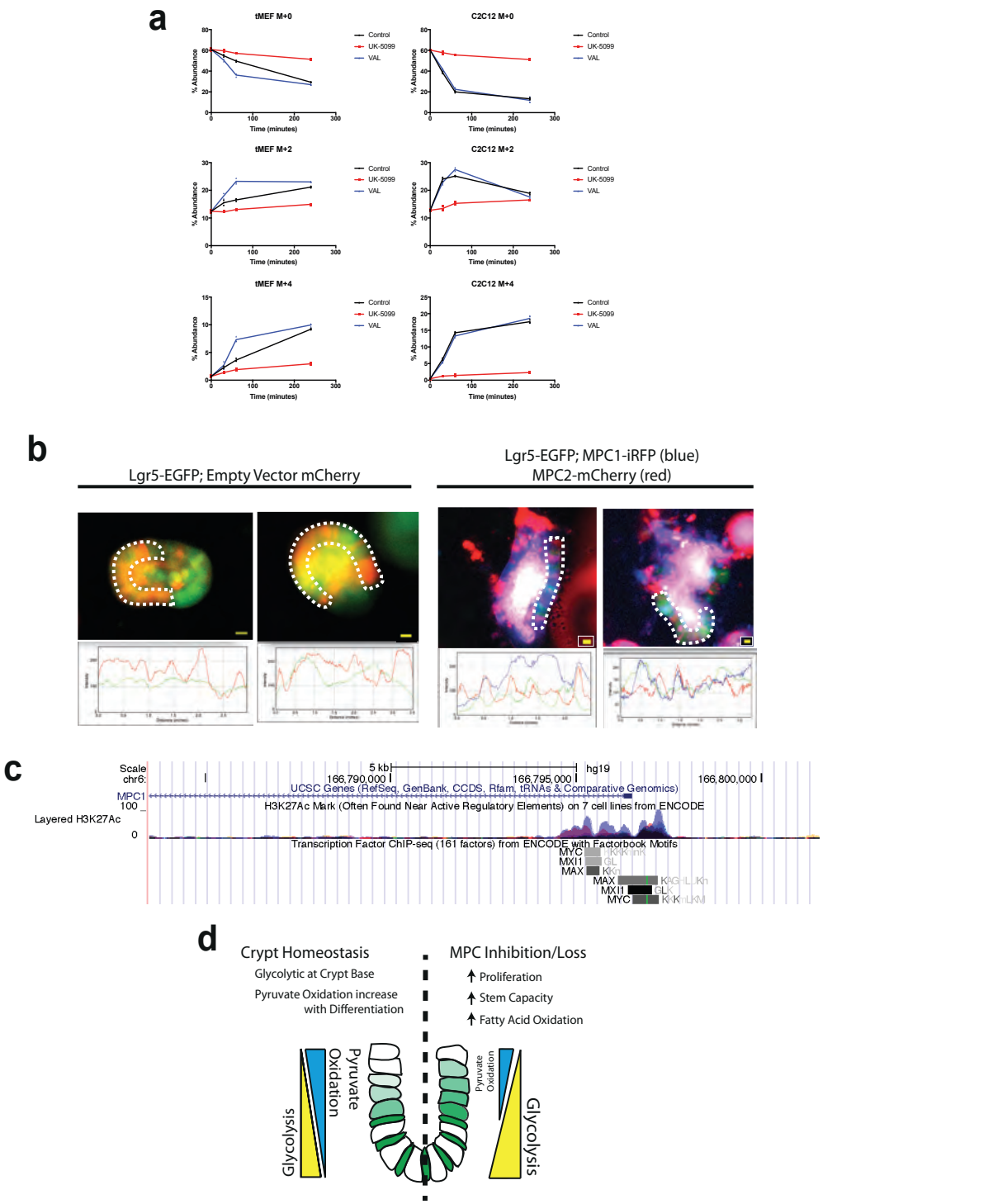

Supplementary Figure 6 Effects of UK-5099 and MPC over expression a, Flux profiling of U-C13 Glucose incorporation into Citrate for tMEF and C2C12 cell lines treated with UK-5099 or Valproic Acid over 4 hours (n = 3 per condition per timepoint). b, Representative images of infected Lgr5-EGFP (green) organoids with either Empty Vector-mCherry (in red) or MPC1-iRFP (in blue) and MPC2 mCherry (in red). Traces below represent intensity of each color over the length of the line outlined by white dotted line in the image. (n = 4 organoids with at least 15 infected cells per organoid counted). c, ENCODE track for Myc and associated transcription factors localized to the Mpc1 promoter. d, Model where crypt homeostasis involves low pyruvate oxidation at the base which increases during differentiation. MPC1 loss leads to reduced pyruvate oxidation, increased glycolysis, increased proliferation, and an expansion of the stem cell compartment within the crypt. Data are mean ± s.e.m. $^{*}P < 0.05$, $^{**}P < 0.01$, $^{***}P < 0.001$. All p values were calculated using Student's t-test.

a

Membrane 1, 2: Secondary (rabbit) 680nm channel

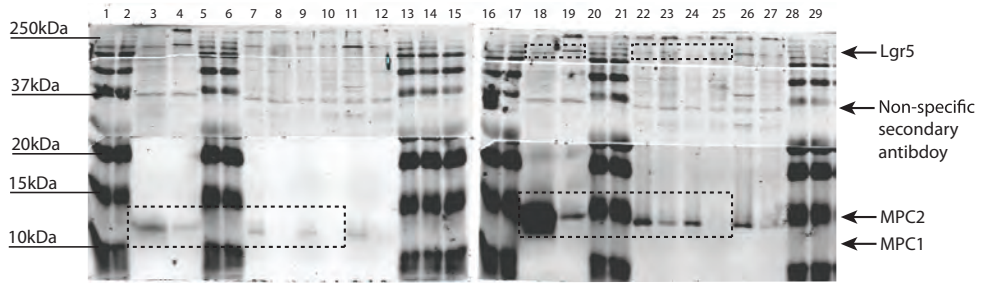

Membrane 1, 2: Secondary (mouse) 800nm channel

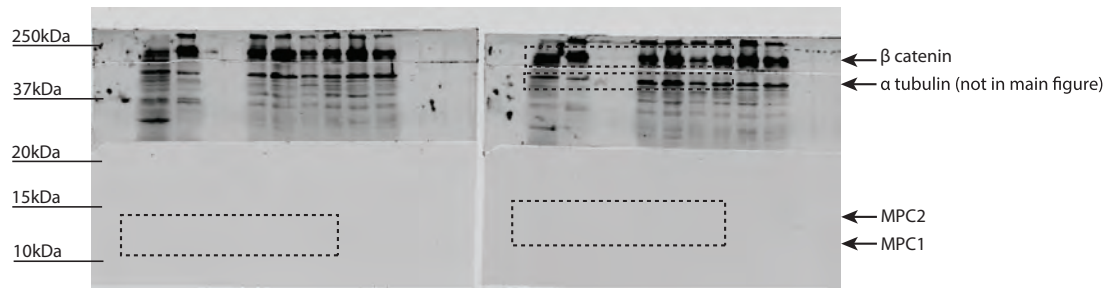

1, 2, 5, 6, 13, 14, 15, 16, 17, 20, 21, 28, 29: Marker
3, 18: Villi
4, 19: Crypt
7, 22: Control 1
8, 23: MPC1 $^{Lgr5\text{-}KO\ 1}$
9, 24: Control 2
10, 25: MPC1$^{Lgr5\text{-}KO\ 2}$
11, 26: Mutated Line B control
12, 27: Mutated Line B MPC1 KO

Membrane 3, 4: Secondary (mouse) 800nm channel

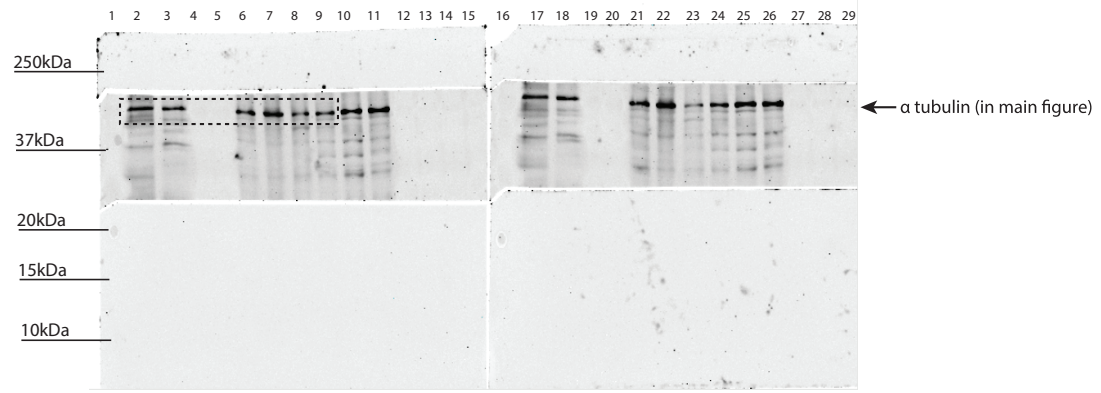

1, 4, 5, 12, 13, 14, 15, 16, 19, 20, 27, 28, 29: Marker
2, 17: Villi
3, 18: Crypt
6, 21: Control 1
7, 22: MPC1$^{Lgr5\text{-}KO\ 1}$
8, 23: Control 2
9, 24: MPC1$^{Lgr5\text{-}KO\ 2}$
10, 25: Mutated Line B control
11, 26: Mutated Line B MPC1 KO

Supplementary Figure 7 Unprocessed western blot membranes. a, Unprocessed western blot images to accompany Figure 5a. b, Unprocessed western blot images to accompany Figure 5b and Supplemental Figure 4e. c, Unprocessed western blot images to accompany Supplemental Figure 2b. d, Unprocessed western blot images to accompany Supplemental Figure 4c.

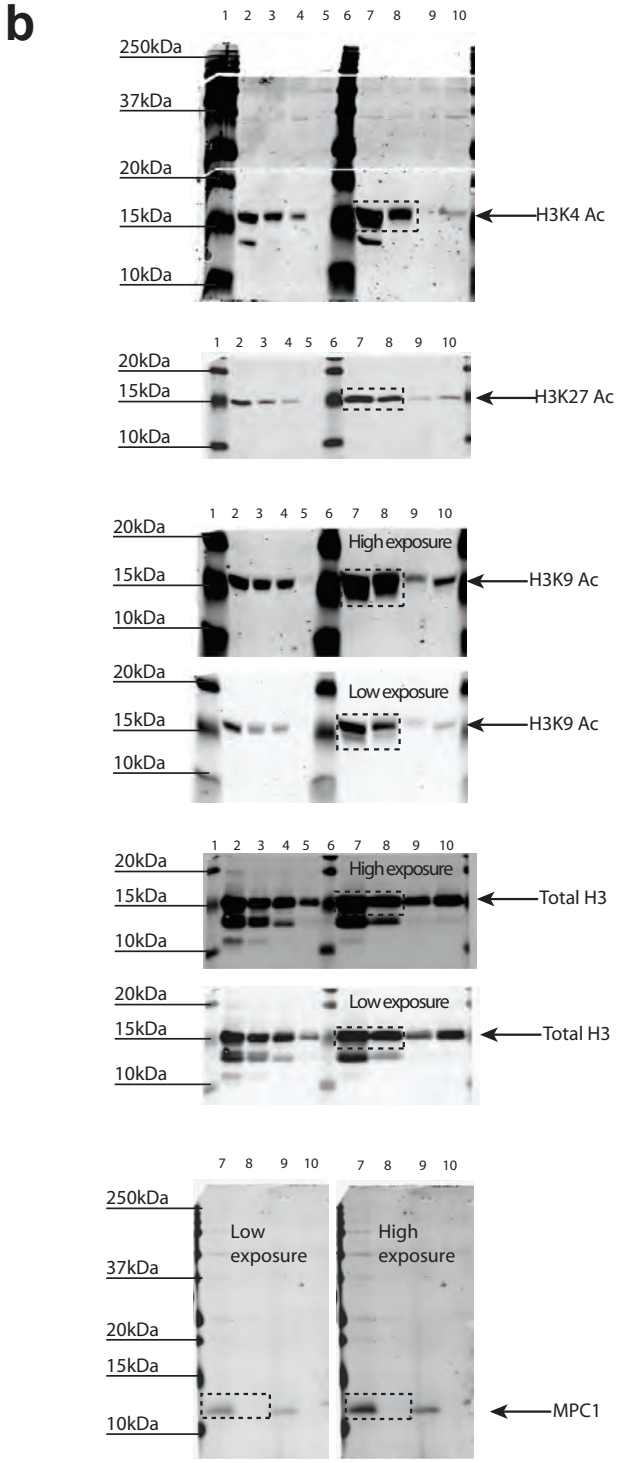

1, 6: Marker
2, 7: Control 1
3, 8: MPC1$^{Lgr5\text{-}KO\ 1}$
4, 9: Control 2
5, 10: MPC1$^{Lgr5\text{-}KO\ 2}$

Supplementary Figure 7 Continued

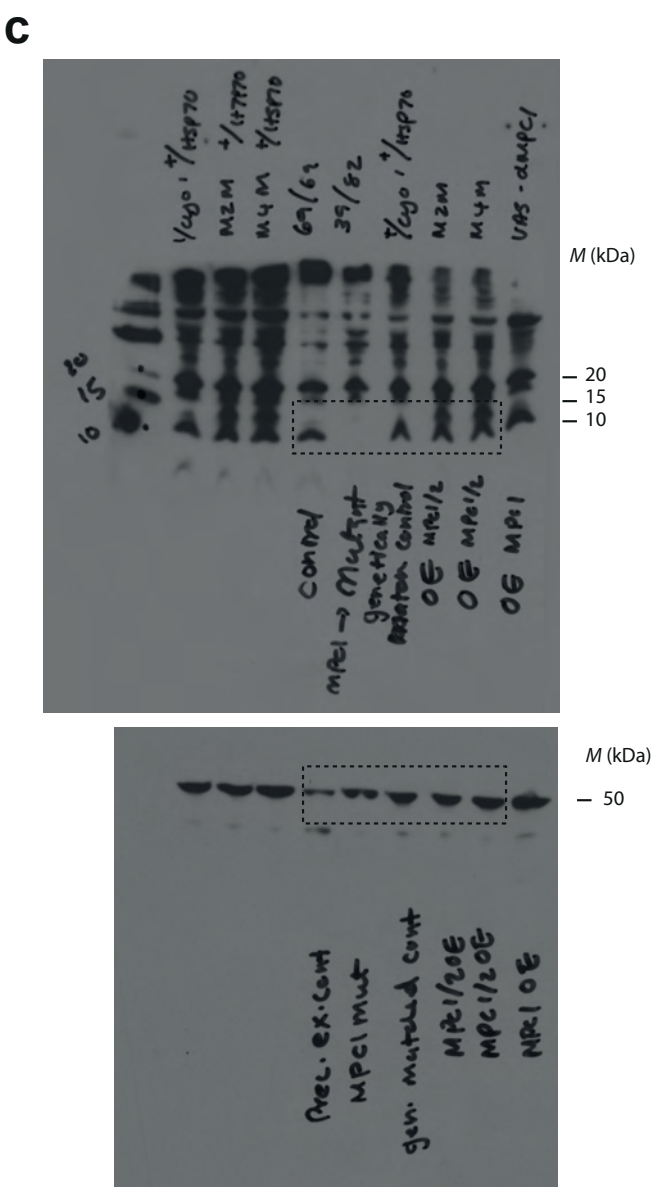

Supplementary Figure 7 Continued

Supplementary Table Legends

Supplementary Table 1 Single cell sort based on EGFP low, mid, and high z-scores for heat map in Figure 1b.

Supplementary Table 2 Transcript z-scores for organoids grown in EN, ENR, and ENR +Wnt3a used to generate heatmap in Figure 1d.

Supplementary Table 3 Transcript z-scores for Lgr5-EGFP Control vs. MPC1-KO organoids used to generate heat map in Supplemental Figure 4d.

Supplementary Table 4 Transcript z-scores for organoids grown in wENR or UK-5099 used to generate the heat map in Figure 6j.

Supplementary Table 5 Information on antibodies used in this work and probe sequences for *in situ* hybridization.

Supplementary Table 6 Nanostring primer design information.

Supplementary Table 7 Statistics Source Data

nature research

Corresponding author(s): Jared Rutter

☐ Initial submission ☐ Revised version ☒ Final submission

Life Sciences Reporting Summary

Nature Research wishes to improve the reproducibility of the work that we publish. This form is intended for publication with all accepted life science papers and provides structure for consistency and transparency in reporting. Every life science submission will use this form; some list items might not apply to an individual manuscript, but all fields must be completed for clarity.

For further information on the points included in this form, see Reporting Life Sciences Research. For further information on Nature Research policies, including our data availability policy, see Authors & Referees and the Editorial Policy Checklist.

Experimental design

1. Sample size

Describe how sample size was determined.

No sample-size calculation was performed. An n of 10 was used for in vivo studies due to the high degree of variability. For in vitro studies a minimum of an n of 3 was used where sample was limiting and if possible an n of 6 was used.

2. Data exclusions

Describe any data exclusions.

No data was excluded from analysis for any reason other than being unusable. For histology this encompasses a lack or heterogeneity of stain or improper section orientation that precluded analysis. For in vitro experiments an unusable sample would be if a sample was lost or not detected in the case of metabolomics.

3. Replication

Describe whether the experimental findings were reliably reproduced.

No attempts at replication of experiments in the paper failed. Data in this paper was reproducible: numbers of experiments and source data has been provided.

4. Randomization

Describe how samples/organisms/participants were allocated into experimental groups.

Animals and in vitro cultures were paired and distributed into control and experimental groups for side-by-side comparison. No formal allocation/ randomization was done; animals were taken as they became available.

5. Blinding

Describe whether the investigators were blinded to group allocation during data collection and/or analysis.

For experiments involving histology animals were allocated into control and experimental. Throughout collection of tissue, sectioning, staining, and analysis researchers were blinded and unblinded only after results had been tabulated. For in vitro cultures, treated organoids were analyzed and quantification of was done before unblinding. Analysis for metabolomics, western blot, flow cytometry was also carried out blinded.

Note: all studies involving animals and/or human research participants must disclose whether blinding and randomization were used.

6. Statistical parameters

For all figures and tables that use statistical methods, confirm that the following items are present in relevant figure legends (or in the Methods section if additional space is needed).

n/a	Confirmed
☐	☒ The exact sample size (*n*) for each experimental group/condition, given as a discrete number and unit of measurement (animals, litters, cultures, etc.)
☐	☒ A description of how samples were collected, noting whether measurements were taken from distinct samples or whether the same sample was measured repeatedly
☐	☒ A statement indicating how many times each experiment was replicated
☐	☒ The statistical test(s) used and whether they are one- or two-sided (note: only common tests should be described solely by name; more complex techniques should be described in the Methods section)
☐	☒ A description of any assumptions or corrections, such as an adjustment for multiple comparisons
☐	☒ The test results (e.g. *P* values) given as exact values whenever possible and with confidence intervals noted
☐	☒ A clear description of statistics including central tendency (e.g. median, mean) and variation (e.g. standard deviation, interquartile range)
☐	☒ Clearly defined error bars

See the web collection on statistics for biologists for further resources and guidance.

Software

Policy information about availability of computer code

7. Software

Describe the software used to analyze the data in this study.	Graphpad Prism 6 was used to analyze and graph data for this work. Types of graphs and tests have been described for all data.

For manuscripts utilizing custom algorithms or software that are central to the paper but not yet described in the published literature, software must be made available to editors and reviewers upon request. We strongly encourage code deposition in a community repository (e.g. GitHub). *Nature Methods* guidance for providing algorithms and software for publication provides further information on this topic.

Materials and reagents

Policy information about availability of materials

8. Materials availability

Indicate whether there are restrictions on availability of unique materials or if these materials are only available for distribution by a for-profit company.	All materials are available from the authors upon request or purchased commercially (vendor and catalog numbers provided).

9. Antibodies

Describe the antibodies used and how they were validated for use in the system under study (i.e. assay and species).	All antibody catalog numbers and dilutions have been provided in Supplementary Table 5. For histology, immunofluorescence, and western blotting positive and negative control samples were used to confirm specificity and validated in the species being tested.

10. Eukaryotic cell lines

a. State the source of each eukaryotic cell line used.	tMEFs were provided by Dean Tantin and C2C12 cells were purchased from ATCC.
b. Describe the method of cell line authentication used.	Cell lines were not authenticated.
c. Report whether the cell lines were tested for mycoplasma contamination.	Cell lines were tested for mycoplasma contamination and found to be negative upon receipt but not tested immediately prior to the experiments in this work.
d. If any of the cell lines used are listed in the database of commonly misidentified cell lines maintained by ICLAC, provide a scientific rationale for their use.	No cell lines used in this work are listed as commonly misidentified by ICLAC. Cell lines used were for basic studies on the ability of Valprioic Acid and UK-5099 to block mitochondrial pyruvate metabolism.

Animals and human research participants

Policy information about studies involving animals; when reporting animal research, follow the ARRIVE guidelines

11. Description of research animals

Provide details on animals and/or animal-derived materials used in the study.

Mice used in this study were purchased from Jackson Labs (Lgr5-EGFP) or generated from ES cells as previously published (Mpc1 fl/fl). For in vivo knockout experiments 6- to 8-week-old mice were used. No formal randomization was performed for animal studies, animals were used as they came available, paired with littermate controls where possible, there was no preference for male or female animals, both genders were included in each analysis. For Drosophila studies, mutant dMPC11 and dMPC12 flies have been previously described (reference 70); RNAi transgenic stocks are as follows: UAS-dMPC1 RNAi and UAS-dMPC2-RNAi, UAS-PDH-E1 (VDRC101856), UAS-PDH-E2 (VDRC 102893), and UAS-Notch-RNAi. All Drosophila studies were done following standard ethical guidelines for working with this organism. As is standard in studies of Drosophila intestinal stem cells, all experiments were performed in females, which have a higher rate of basal stem cell proliferation than males. Experiments were conducted in adults aged four days to three weeks after eclosion.

Policy information about studies involving human research participants

12. Description of human research participants

Describe the covariate-relevant population characteristics of the human research participants.

During colonoscopy a biopsy or tissue was collected from the Ascending Colon. This was used to liberate crypts as previously described for in vitro growth assays in different drug treatment conditions. Biopsies were collected from healthy female patients undergoing routine colonscopy between the ages of 51-60.

nature research

Corresponding author(s): Jared Rutter

☐ Initial submission ☐ Revised version ☒ Final submission

Flow Cytometry Reporting Summary

Form fields will expand as needed. Please do not leave fields blank.

Data presentation

For all flow cytometry data, confirm that:

☒ 1. The axis labels state the marker and fluorochrome used (e.g. CD4-FITC).

☒ 2. The axis scales are clearly visible. Include numbers along axes only for bottom left plot of group (a 'group' is an analysis of identical markers).

☒ 3. All plots are contour plots with outliers or pseudocolor plots.

☒ 4. A numerical value for number of cells or percentage (with statistics) is provided.

Methodological details

5. Describe the sample preparation.	Crypts were isolated from mice as described or organoids were dissociated from matrigel. Single cells were purified by TrypLE and DNase treatment, flitered, and resuspended in basal media. DAPI was used as an additional live/dead stain or gating was based on cell size to exclude debris and exclude doublets.
6. Identify the instrument used for data collection.	BD Canto and BD FACS Aria
7. Describe the software used to collect and analyze the flow cytometry data.	BD FACSDIVA and FlowJo v.10
8. Describe the abundance of the relevant cell populations within post-sort fractions.	Populations of GFP positive cells (low mid and high) resulting from mice were between 0.5 and 5%. GFP positive cells from in vitro organoids ranged from 3.9 to 40% depending on experimental condition.
9. Describe the gating strategy used.	Side Scatter and forward scatter area were used as an initial gate for cell debris and aggregates. Side scatter height by side scatter width followed by forward scatter height by forward scatter width were used to isolate singlets. Gating for GFP positive cells was set in reference to a negative wild-type control culture. GFP high, mid, and low population gates were set to allocate approximately 1/3 of the positive cells in each group for collection. An exemplar of this gating strategy is shown in Supplemental Figure 1a.

Tick this box to confirm that a figure exemplifying the gating strategy is provided in the Supplementary Information. ☒